Boston University

College of Engineering

Thesis

AN ULTRA-FAST DIGITAL DIFFUSE OPTICAL SPECTROSCOPIC IMAGING SYSTEM FOR NEOADJUVANT CHEMOTHERAPY MONITORING

by

ALYSSA TORJESEN

B.S., Pepperdine University, 2010

Submitted in partial fulfillment of the

requirements for the degree of

Master of Science

2016

Approved by

First Reader

_____

Darren Roblyer, Ph.D.
Assistant Professor of Biomedical Engineering

Second Reader

_____

Irving Bigio, Ph.D.
Professor of Biomedical Engineering
Professor of Electrical and Computer Engineering

Third Reader

_____

Sergio Fantini, Ph.D.
Professor of Biomedical Engineering
Tufts University

Acknowledgements

I would like to thank my advisor, Dr. Darren Roblyer, who sparked my interest in the world of diffuse optics. He has skillfully explained countless concepts to me about instrumentation and optics and has guided me through numerous design challenges with great patience. His passion for advancing optical technologies and improving cancer care is evident in his dedication to his students and research, and I am very fortunate to have been mentored by such an exceptional advisor.

I am grateful for the many contributions from the fellow graduate students in the Biomedical Optical Technologies Lab, including Raeef Istfan, Kavon Karrobi, Hannah Peterson, Syeda Tabassum, Fei Teng, and Yanyu Zhao. I am particularly grateful for Raeef's help with instrumentation and Hannah's help with measurements and data processing.

Those who have worked on the dDOSI project before me have laid the groundwork for a successful and powerful clinical instrument. I would like to thank Justin Jung, who studied undersampling as a viable direct sampling method for the dDOSI system. The 2013 Senior Design Group was instrumental in providing the hardware-integrated platform that is the basis of the dDOSI system. Finally, I would like to acknowledge all the hard work and patience of the members of the Electronics Design Facility, particularly Dan Gastler and Dean

DeCarli, who have helped with troubleshooting hardware challenges and with countless iterations of the firmware to perfect all signal generation and sampling.

I am grateful for my colleagues' dedication to improving health that has allowed this project to be successful, and for the unconditional support of my family that has driven me to pursue my goals.

AN ULTRA-FAST DIGITAL DIFFUSE OPTICAL SPECTROSCOPIC IMAGING SYSTEM FOR NEOADJUVANT CHEMOTHERAPY MONITORING

Abstract

Up to 20% of breast cancer patients who undergo presurgical (neoadjuvant) chemotherapy have no response to treatment. Standard-of-care imaging modalities, including MRI, CT, mammography, and ultrasound, measure anatomical features and tumor size that reveal response only after months of treatment. Recently, non-invasive, near-infrared optical markers have shown promise in indicating the efficacy of treatment at the outset of the chemotherapy treatment. For example, frequency domain Diffuse Optical Spectroscopic Imaging (DOSI) can be used to characterize the optical scattering and absorption properties of thick tissue, including breast tumors. These parameters can then be used to calculate tissue concentrations of chromophores, including oxyhemoglobin, deoxyhemoglobin, water, and lipids. Tumors differ in hemoglobin concentration, as compared with healthy background tissue, and changes in hemoglobin concentration during neoadjuvant chemotherapy have been shown to correlate with efficacy of treatment. Using DOSI early in treatment to measure chromophore concentrations may be a powerful tool for guiding neoadjuvant chemotherapy treatment.

Previous frequency-domain DOSI systems have been limited by large device footprints, complex electronics, high costs, and slow acquisition speeds, all

of which complicate access to patients in the clinical setting. In this work a new digital DOSI (dDOSI) system has been developed, which is relatively inexpensive and compact, allowing for use at the bedside, while providing unprecedented measurement speeds. The system builds on, and significantly advances, previous dDOSI setups developed by our group and, for the first time, utilizes hardware-integrated custom board-level direct digital synthesizers (DDS) and analog to digital converters (ADC) to generate and directly measure signals utilizing undersampling techniques. The dDOSI system takes high-speed optical measurements by utilizing wavelength multiplexing while sweeping through hundreds of modulation frequencies in tens of milliseconds. The new dDOSI system is fast, inexpensive, and compact without compromising accuracy and precision.

Contents

List of Figures

List of Tables

Background

Motivation

Breast cancer is the most commonly occurring cancer in the United States, making up 14.6% of all cancer diagnoses[1]. A growing number of breast cancer patients undergo neoadjuvant chemotherapy (NAC) prior to mastectomy or lumpectomy in an effort to eliminate or reduce the size of the tumor and allow for a less invasive surgery. NAC response is typically categorized into three response groups—pathological complete response (pCR), partial response (PR), and no response (NR), where those with a pCR or PR tend to have increased long term survival[2], [3]. About 9-20% of women who undergo NAC fall into the NR group[4], [5], which can mean receiving months of toxic drugs with no reduction in tumor dimension.

Current standard of care breast cancer structural imaging modalities include x-ray mammography[6], MRI[6], [7], and ultrasound[6]. Each of these modalities has unique benefits in determining the location or morphology of the tumor, but it typically takes weeks to months of treatment to identify structural and anatomic changes in the tumor. Thus, a patient may undergo most or all of a NAC regimen before structural imaging would provide information as to whether or not the regimen is effective for that particular patient. Alternatively, functional imaging may allow for earlier time point detection of changes in the molecular makeup or metabolism of the tissue. PET-CT is a functional imaging method sometimes employed in breast cancer monitoring, but it requires an exogenous

contrast agent which can be harmful to the patient. Diffuse optical imaging, instead, uses only non-ionizing radiation and can recover information about metabolism and chromophore concentrations, such as oxy- or deoxy-hemoglobin, water, and lipid, in the tumor and surrounding tissue, making it possible to differentiate breast tumors from healthy tissue[8], [9].

Previous studies have shown changes in chromophore concentrations in the first days or weeks of NAC may be predictive of pathological response. Cerussi *et al*[10] and Soliman *et al*[8] showed that a drop in deoxyhemoglobin concentration in the affected breast in the first weeks of therapy was associated with improved pathological response. Later, Roblyer *et al*[11] saw an increase in oxyhemoglobin on the first day of treatment associated with pCR. Although the exact mechanism by which an increase in oxyhemoglobin in the first days of treatment affects NAC response warrants further investigation, the ability to detect chromophore concentrations at early time points in therapy may allow for individual NAC regimens to be altered as needed to provide the most effective treatment for each patient, minimizing unnecessary adverse side effects and improving long term survival.

Diffuse Optical Spectroscopic Imaging Theory

Diffuse Optical Spectroscopic Imaging (DOSI) has been developed over the past three decades to characterize optical scattering and absorption and, in turn, calculate chromophore concentrations in thick tissue[12], [13]. Diffuse

optical imaging is categorized into three distinct measurement types: time domain, frequency domain, and continuous wave. Time domain measurements recover the most information about the tissue, but require complex instrumentation that comes at a high cost. Continuous wave measurement is the simplest of the diffuse optical techniques but, in turn, recovers the least information about the tissue. Frequency domain diffuse optical imaging is a compromise between the other measurement types in that it recovers more information about the tissue than does continuous wave, yet the instrumentation is simpler compared to that required for time domain measurements. This work focuses on frequency domain DOSI to recover tissue optical properties.

As photons travel through tissue, they undergo both absorption by chromophores and scattering when encountering changes in refractive index. Both scattering and absorption attenuate the measured intensity of light at the detector position, which poses difficulties in separating the individual effects of each. Absorption is wavelength-dependent for each chromophore, as shown in Figure 1[14], while scattering

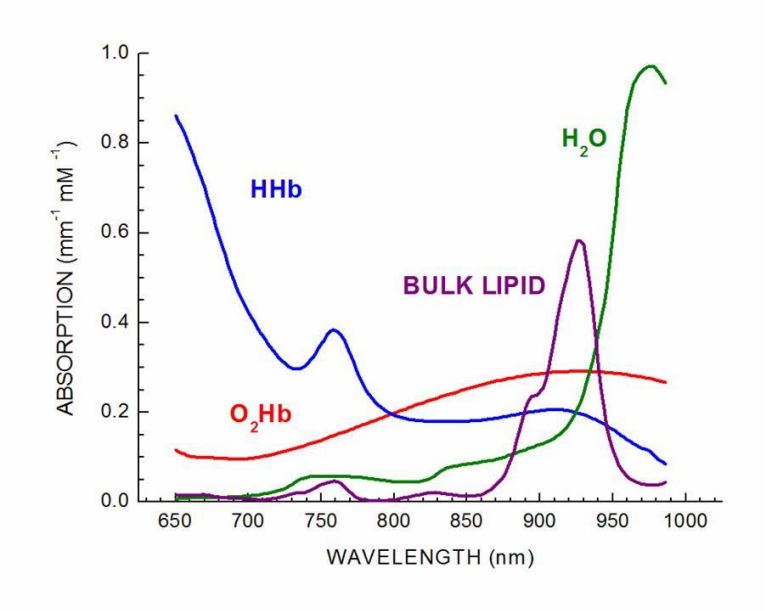

Figure 1. Absorption spectra of common biological absorbers in the near infrared. Water and lipid values have been rescaled.

decreases with increasing wavelength in a power law relationship in the NIR[15].

Given the high scattering of light in most human tissues (μ_s' is typically at least 10 fold higher than μ_a in the near-infrared [NIR]), photon propagation can be modeled using the Boltzmann Transport Equation[13], [16]. Analytical solutions to the Boltzmann Transport Equation are non-trivial, and the equation is often simplified to the time-dependent standard diffusion equation, also called P1 approximation [17],

$$\frac{1}{c}\frac{\partial\varphi(\boldsymbol{r},t)}{\partial t} - D\nabla^2\varphi(\boldsymbol{r},t) + \mu_a\varphi(\boldsymbol{r},t) = S(\boldsymbol{r},t) \qquad (1)$$

where φ is the fluence rate, S is the source, c is the speed of light in tissue, and

$$D = \frac{1}{3(\mu_a+\mu_s')} \quad . \qquad (2)$$

The diffusion approximation can also be formulated for a point source sinusoidally modulated at angular frequency, ω, [17]

$$\varphi(\boldsymbol{r},t) = \frac{A_{dc}}{4\pi D}\frac{exp(-\frac{r}{\delta})}{r} + \frac{A_{ac}}{4\pi D}\frac{exp(-k_{real}r)}{r} \times exp[-i(k_{imag}r - \omega t)] \ , \qquad (3)$$

where A_{dc} is the DC component of the source, A_{ac} is the AC component of the source, δ is the DC penetration depth, and k_{real} and k_{imag} are the real and imaginary parts of the photon density wave vector, respectively, which are defined as

$$k_{real} = \sqrt{\frac{3}{2}\mu_a\mu_s'}\{[1 + \left(\frac{\omega}{c\mu_a}\right)^2]^{\frac{1}{2}} + 1\}^{1/2} \qquad (4)$$

and

$$k_{imag} = \sqrt{\frac{3}{2}\mu_a\mu_s'}\{[1 + \left(\frac{\omega}{c\mu_a}\right)^2]^{\frac{1}{2}} + 1\}^{1/2} \quad . \qquad (5)$$

Boundary conditions must be carefully considered in order to avoid discontinuities at the air-tissue boundary. For a source-detector geometry in reflectance mode with boundary conditionsdescribing a semi-infinite medium [17], [18], the measured phase lag and amplitude attenuation are defined as

$$\theta_{lag(\rho,\omega)} = k_{imag}(\omega) r_0 - arctan(\frac{IMAG}{REAl}) \quad (6)$$

and

$$A_{att}(\rho,\omega) = \frac{A_{ir}}{4\pi D}(REAL^2 + IMAG^2)^{1/2} \quad , \quad (7)$$

where

$$REAL = \frac{exp[-k_{real}(\omega) r_{0b}]}{r_{0b}} - cos[k_{imag}(\omega)(r_{0b} - r_0)] \frac{exp[-k_{real}(\omega) r_{0b}]}{r_{0b}} \quad (8)$$

$$IMAG = sin\left[k_{imag}(\omega)(r_{0b} - r_0)\right] \frac{exp[-k_{real}(\omega) r_{0b}]}{r_{0b}} \quad (9)$$

$$r_0 = [(\mu_s')^{-2} + \rho^2]^{1/2} \quad (10)$$

$$r_{0b} = [\left(\frac{4}{3\mu_{s'}} \frac{1+R_{eff}}{1-R_{eff}} + \frac{1}{\mu_{s'}}\right)^2 + \rho^2]^{1/2} \quad . \quad (11)$$

A_{ir} is the amplitude response of the instrument, and R_{eff} is the effective reflection coefficient[17].

A frequency domain DOSI measurement directly measures the amplitude attenuation and phase delay induced on the photon density waves by the tissue and by the instrument. In order to separate the instrument response from the tissue response, an additional measurement must be taken on a phantom with known optical properties. The known optical properties (obtained from multi-distance measurements) are used in a forward model, where theoretical amplitude and phase are calculated according to equations 6 and 7. The theoretical amplitude and phase at each modulation frequency are compared,

ratiometrically or differentially, respectively, to the measured amplitude and phase in order to calculate calibration factors[17], [19]. These calibration factors are applied to the amplitude and phase from the tissue measurement, then the calibrated amplitude and phase are used in an inverse model, according to equations 6 and 7, where least-squares fitting is used to find μ_a and μ_s' at each wavelength by incrementally updating initial guesses for μ_a and μ_s' until the error is minimized[17]. A modified Beer-Lambert law[20],

$$\overrightarrow{\mu_a}(\lambda) = 2.303[\varepsilon(\lambda)]\vec{C} \quad (12)$$

relates μ_a to chromophore concentrations, where ε(λ) is the wavelength-specific extinction coefficient and C is chromophore concentration. A system of linear equations is used to determine concentrations of each chromophore of interest, based on calculated μ_a values and extinction coefficients from Zijlstra *et al* [21].

Instrumentation

Frequency domain DOSI may be approached by using either a single modulation frequency[22]–[27] or a sweep of multiple frequencies[17], [19], [28] in the radio frequency (RF) range. Measurement of RF signals is challenging given the high speed of the signals; therefore, most single modulation frequency systems utilize either homodyne[23], [25], [27], [28] or heterodyne[22] techniques to down-convert the high frequency signal of interest by mixing it with a reference signal. Broad bandwidth DOSI instruments[12], [29] that utilize light sources modulated at numerous RF frequencies have met such challenges using a

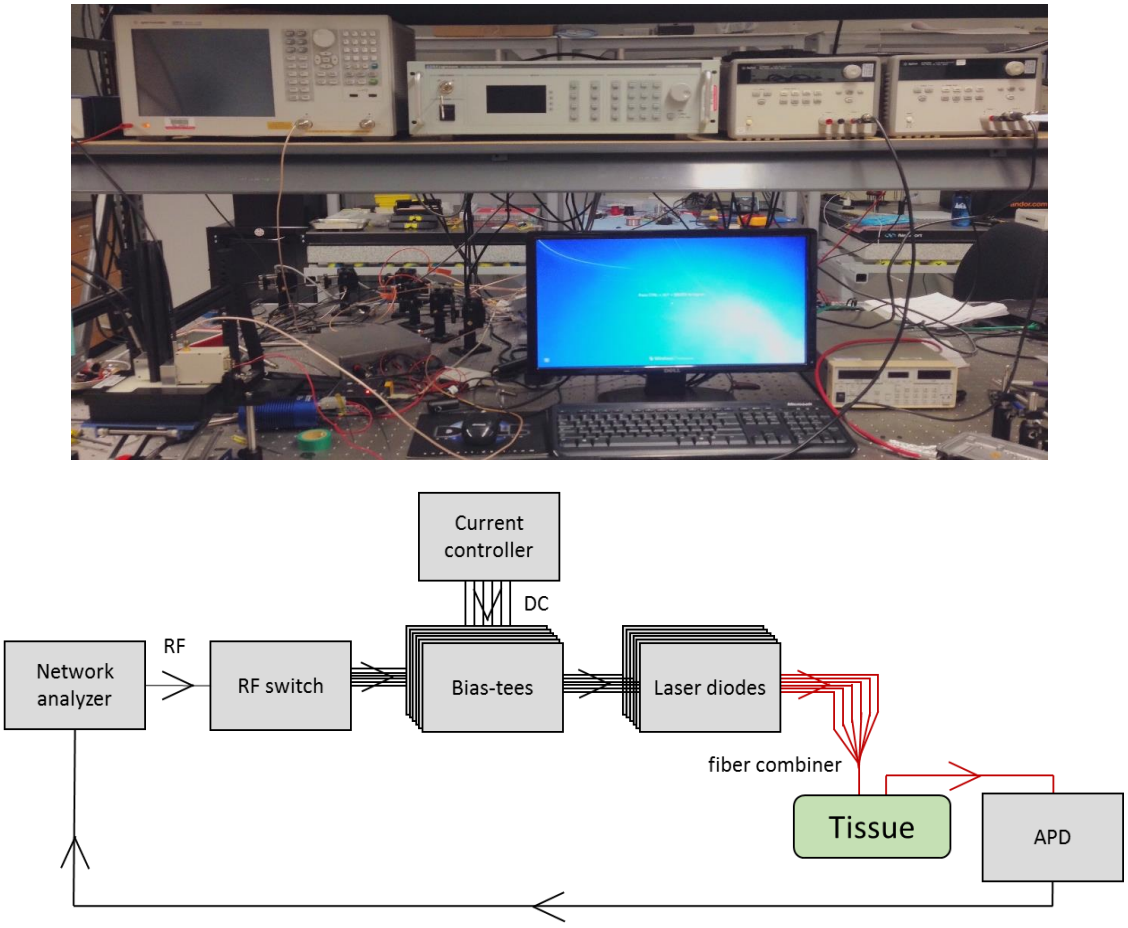

Figure 2. Benchtop DOSI overview and schematic.

network analyzer—a benchtop instrument that generates and detects electrical signals up to the gigahertz range. Network analyzers are accurate and precise, but they are also expensive and have relatively large instrument footprints. A schematic of a network analyzer-based frequency domain DOSI system is shown in Figure 2, which will be considered the gold-standard instrument, referred to as the “benchtop DOSI system”, in this work. The size of such a system can be prohibitive to accessing patients in the clinic, and the cost can range from $30,000 to $60,000 (based on our internal cost estimates). Although some analog systems have been miniaturized[20], [30], the highly sensitive RF circuitry makes implementation and repairs difficult. Furthermore, frequency domain DOSI

instruments are typically slow in acquisition time compared to their CW counterparts, often requiring minutes to acquire a full set of data, for example, using multiple wavelengths modulated at a single frequency and measured at multiple detectors[27]. Although recent improvements have been made in data acquisition rates for single modulation frequency measurements[24], frequency sweep DOSI systems typically require 10s of seconds to acquire data at all wavelengths and modulation frequencies. A high-speed, broad-bandwidth, digital, miniaturized DOSI system would simplify the analog circuitry, while also reducing the cost and footprint of the device, enabling access to more patients in the clinic or infusion suite.

In order to create a digital system, both the signal generation and detection functionalities of the network analyzer must be replaced. Past work has demonstrated the feasibility of digital signal generation and detection using direct digital synthesizer (DDS) integrated circuits to generated RF signals and a 3.6 gigasample per second 2-channel analog to digital converter (ADC)[31]. This system relied on manufacturer evaluation boards to control the DDS and ADC chips, resulting in slow communication between the hardware and control software. Furthermore, the high sampling rate of the ADC resulted in lengthy data transfer times. A second implementation of a digital system tested the feasibility of utilizing a slower ADC, sampling at only 25 megasamples per second[32]. Although signals were generated at up to 400 MHz, undersampling was successfully employed; given that the modulation frequency was always known, the aliased signal could be identified in the baseband. This

implementation, again, relied on manufacturer evaluation boards, and a measurement consisting of a frequency sweep at a single wavelength took 8 minutes. In order for a digital DOSI (dDOSI) system to be practical for clinical measurements, data acquisition rates must be drastically increased, all hardware components must be fully integrated, and the overall footprint and cost of the device must be reduced.

Specific Aims

Aim 1: Complete system design and fabrication of hardware and software for high-speed dDOSI system. A custom motherboard containing a 2-channel 250 mega-sample per second (MSPS) ADC and DDS daughterboards were previously designed and fabricated by our group. These boards require testing and integration with optical components, RF components, and user software prior to clinical use. The instrument will utilize wavelength multiplexing, such that lasers (up to 6 spanning the NIR) can be modulated simultaneously and frequencies between 50 and 400 MHz can be swept. A Matlab-based graphical user interface will allow the user to set modulation parameters, iterate measurements, and visualize amplitude and phase data. Algorithms will be implemented to process multiplexed amplitude and phase data.

Aim 2: Quantify dDOSI performance compared with gold-standard system. Signal-to-noise ratio and measurement acquisition timing will be determined for the dDOSI system. Precision over time will be determined by performing drift tests, and dDOSI accuracy will be compared with that of a gold-standard benchtop DOSI system. Tissue-simulating phantom optical properties will be extracted and compared with those taken at comparable wavelengths and modulation frequencies using the benchtop DOSI system.

Aim 3: Validate *in vivo* measurement performance. Forearm cuff occlusion measurements will be used to determine the ability of the dDOSI system to detect changes in oxyhemoglobin and deoxyhemoglobin concentrations. Given that the

dDOSI system will acquire measurements at a rate of tens of milliseconds per acquisition, it will be determined if there are detectable changes in optical properties and chromophore concentrations throughout the cardiac cycle. Finally, measurements will be taken on a healthy volunteer to ensure that physiologically relevant chromophore values can be extracted in the breast.

Aim 1 Results: System Development

The dDOSI system has been designed such that high-speed, broad bandwidth, frequency domain measurements can be taken using digital signal generation and detection, allowing for improved system portability and lower instrument cost. The current implementation of the dDOSI instrument consists of six laser diode wavelengths spanning the NIR range, utilizing either compact, fiber-coupled laser diode modules or lager, fan-cooled laser diode modules. Lasers are driven with a DC current generated either by miniaturized current

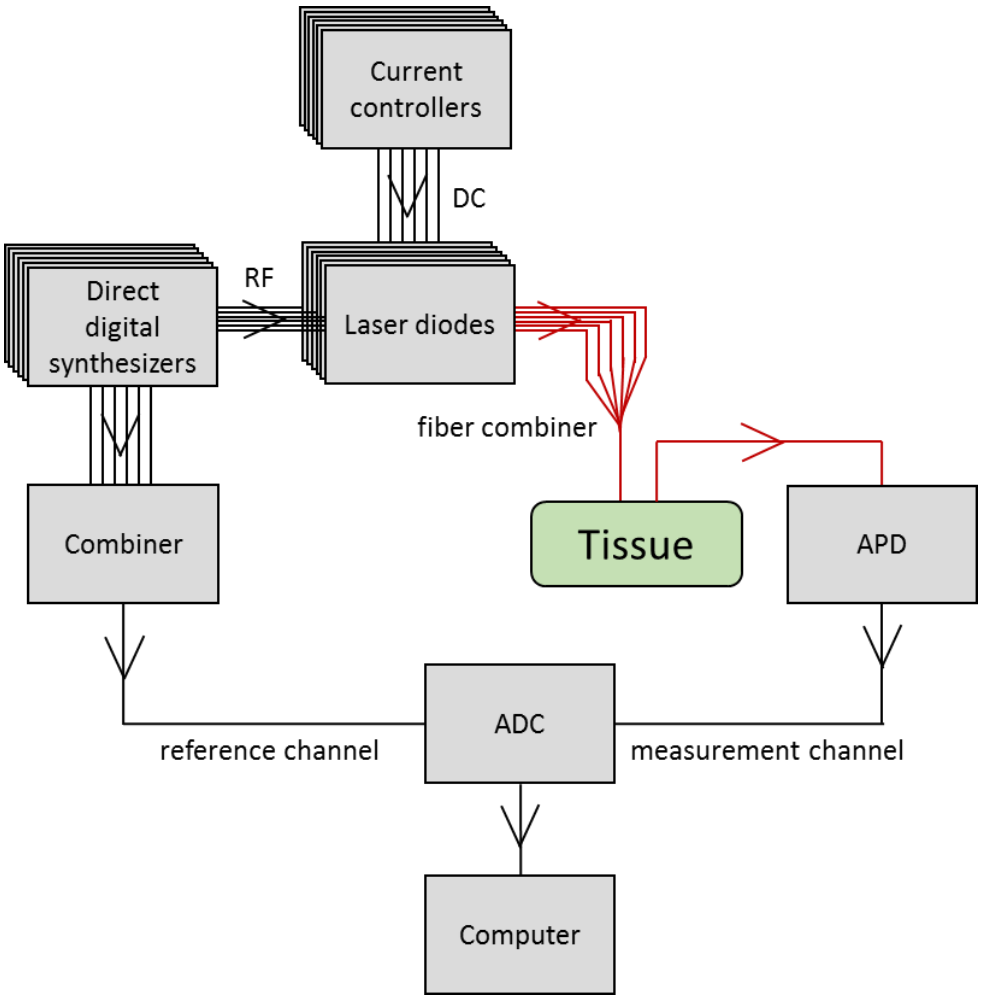

Figure 3. dDOSI system schematic.

source modules or by a standard, precision current controller. Light sources are modulated simultaneously with RF currents up to 400 MHz generated by DDS boards. The multiplexed optical signals are detected with an avalanche photodiode (APD), and a 2-channel ADC samples the electrical output of the measurement and reference channels at 250 MSPS. A schematic of the system is shown in Figure 3 and will be explained in detail in the following sections.

Figure 4. dDOSI system core electronics.

Hardware Integration

Previous implementations[31], [32] of the dDOSI system utilized evaluation boards to control the DDS and ADC chips, which resulted in inefficient software-hardware communication and slow measurements. In 2013 the core electronics of the dDOSI system (Figure 4) were integrated into a single motherboard to generate and sample RF signals and to communicate with and transfer data to the host computer, as outlined in Figure 5. A development board (ZedBoard, MircoZed Zynq-7010 SoC) contains an ARM Cortext-A9 processor in an Artix 7 FPGA fabric, 1 GB of RAM to store data read from the ADC, and a Linux server to transfer data between the board and host computer. The user sets the desired frequency sweep settings in

software and the Linux server configures the DDS boards accordingly. The two-channel ADC samples data simultaneously and transfers data to the RAM on the MicroZed module via a parallel low voltage differential signal bus. Data are then transferred from the Linux server to the host computer via an Ethernet link at a rate of up to 170 Mbps. This fully integrated hardware system allows for rapid data acquisition such that fast physiological changes can be detected with the dDOSI system. The primary hardware is housed in a box measuring 10x12x6 inches.

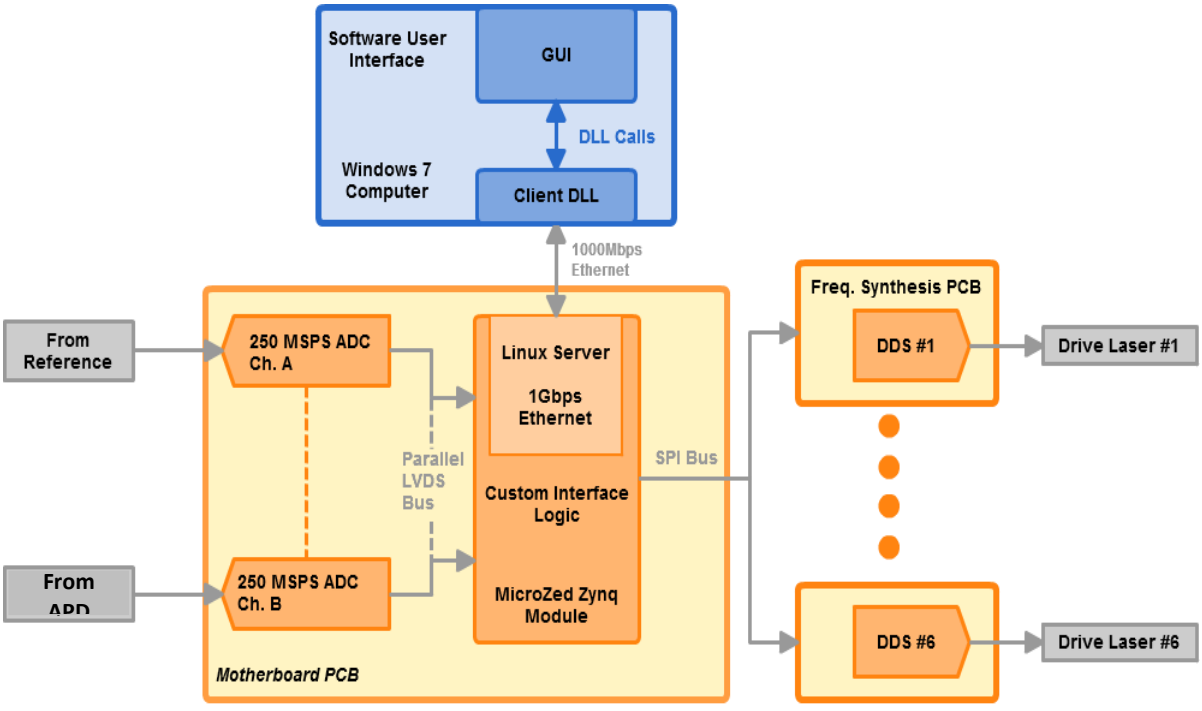

Figure 5. dDOSI hardware overview. Image provided by 2013 senior design group.

Sources

The dDOSI system utilizes NIR laser diodes with wavelengths of 658, 690, 785, 808, 830, and 850 nm. Blood is a primary absorber in biological tissue, and given that the absorption of oxy- and deoxyhemoglobin are low in the NIR region compared with other wavelengths (Figure 1), NIR light is able to propagate relatively deep into tissue. The particular wavelengths used in the dDOSI system allow for accurate recovery of oxy- and deoxyhemoglobin concentrations, however in order to reliably measure other chromophores, such as water or lipid, additional laser diodes should be added near the water (970 nm) and lipid (920 nm) peaks in the absorption spectrum. The dDOSI system utilizes either miniaturized laser diode modules (Blue Sky Research, Fibermax) that are portable for clinical use, or larger laser diode modules (ThorLabs, LDM9T) typically employed with the benchtop DOSI system. All laser diodes are coupled to a single fiber bundle consisting of 400 μm fibers in a single housing.

Each laser diode is driven with a DC current, which is mixed with an RF current at a bias-tee to modulate the light. The DC current source used with the

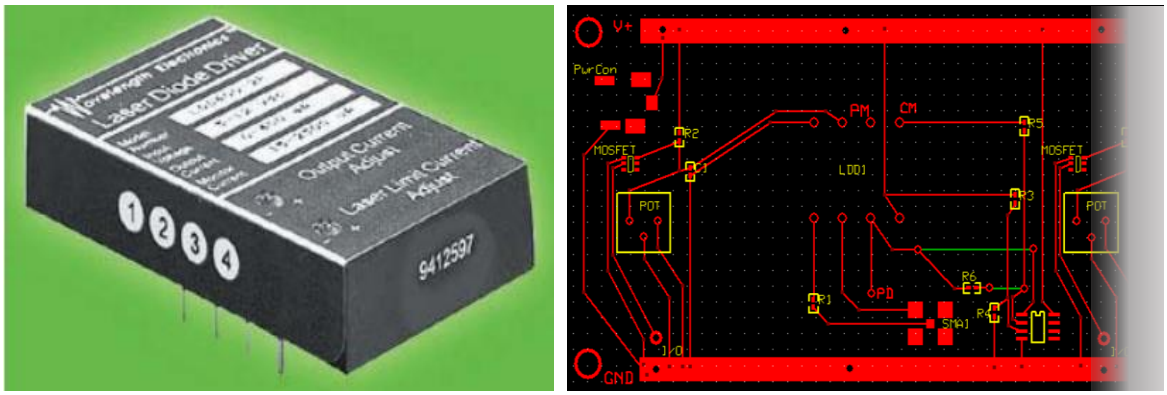

Figure 6. Miniature current controller module and example of custom PCB used to control a single module. The complete PCB controls all six current controller modules.

Laser Diode Driver Specifications	
Current output	0 to 200 mA
Supply voltage	+5 to +12 V
Noise and ripple (rms)	< 5 µA
Power dissipation, 25˚C	1 W

Table 1. Miniaturized laser diode driver specifications

benchtop DOSI system is an 8-channel, high-stability laser diode controller (ILX Lightwave, LDC-390, Newport Corporation). The fully miniaturized dDOSI system utilizes smaller laser diode driver modules (LDD200-2P, Wavelength Electronics, Bozeman, MT, Figure 6) that can output up to 200 mA DC current and be easily incorporated to the dDOSI housing for portability in the clinical setting. Additional specifications for the miniaturized laser diode driver modules are shown in Table 1. Custom printed circuit boards (PCB) were designed to control the miniaturized laser diode driver modules, as shown in Figure 6. Each laser diode driver module contains a modulation input pin, which allows the output current to vary inversely with the voltage applied to the modulation input pin. The voltage to the modulation input pin is set by a simple voltage divider circuit. The custom PCB contains a MOSFET-controlled circuit which allows the current to switch from a warming current (10 mA) to a lasing current (50-100 mA, wavelength dependent)

using a digital I/O controlled in software. The setup for the fully miniaturized dDOSI incorporates both the miniaturized current controller modules and the miniaturized laser diode modules. Some data were collected with the fully miniaturized system, however the majority of the dDOSI measurements presented will utilize the ILX Lightwave laser diode driver and the benchtop lasers, unless otherwise noted. Further investigation into safety components to protect the laser diodes from transient currents will allow for future implementation of the fully miniaturized system.

Modulation

In frequency domain DOSI measurements, each laser diode must be temporally intensity modulated in the RF range. The benchtop DOSI system relied on a network analyzer (Agilent Technologies, E5061B ENA Series) to output RF current in discrete steps from 50 to 500 MHz to modulate each laser diode. The dDOSI system replaces the RF current output functionality of the network analyzer by implementing six DDS chips (AD9910, Analog Devices) on individual daughterboards.

DDS Specifications	
Max internal clock speed	1 GSPS
External clock speed	25 MHz
Max analog output frequency	400 MHz
Frequency resolution	0.23 Hz
DAC bit-depth	14
Typical full-scale output current	20 mA
Power consumption	715 mW

Table 2. Direct digital synthesizer (DDS) specifications.

Manufacturer specifications of DDS chips are presented in Table 2. Each DDS can output up to 20 mA of current modulated up to 400 MHz. In the dDOSI

system, the modulation frequencies utilized are typically between 50 and 300 MHz or between 50 and 400 MHz, depending on the optical attenuation of the sample (higher modulation frequencies may be lost in the noise floor in more attenuating samples) and data acquisition rate requirements. The frequency step size can be set between 1 MHz and 7 MHz. For high speed measurements, the user may choose 7 MHz steps to optimize the temporal resolution of frequency sweeps, or for slower measurements the user may choose 1 MHz steps to optimize frequency resolution.

A primary benefit of using DDS boards instead of the network analyzer as the RF current source is the ability to multiplex the laser diodes. The network analyzer has a single output channel, such that when using the benchtop DOSI system each laser is switched on sequentially and frequency sweeps are performed individually at each wavelength. This results in a total measurement time of approximately 10-15 seconds to modulate 6 lasers diodes at all frequencies of interest, where much of the measurement time is spent on switching between lasers. In contrast, since there are 6 individual DDS chips in the dDOSI system, laser diodes are turned on simultaneously and modulated at offset frequencies. The multiplexed data is then decoupled in the frequency domain. A typical dDOSI measurement, for example, may sweep through frequencies between 50 and 400 MHz in steps of 1 MHz with the modulation frequency for each wavelength offset by 10 MHz. This multiplexing reduces measurement speed to typically less than 100 ms per frequency sweep, allowing for detection of rapid physiological changes.

The RF current output of each DDS board is low-pass filtered at 400 MHz then routed to a 7:1 directional coupler. The majority of the output from the directional coupler is routed to a bias tee where it is combined with the DC current, such that the RF current with a DC offset is used to drive the laser. The lesser output from each directional coupler is used as a reference channel. All reference channels are routed to a power splitter/combiner (Mini-Circuits, ZBSC-615+), such that all reference channels are detected simultaneously at one channel of the ADC.

Detection

The standard dDOSI configuration is a reflectance mode measurement (Figure 7) with the source fiber bundle and active area of an APD placed directly on the surface of the tissue or phantom at a source detector separation of 15 to 30 mm. The APD module (Hamamatsu C5658) has a 0.5 mm active area, 2.50 x 10^5 V/W photoelectric sensitivity, and a high band cutoff of 1 GHz, and contains a bias power supply and low-noise amplifier within a compact package.

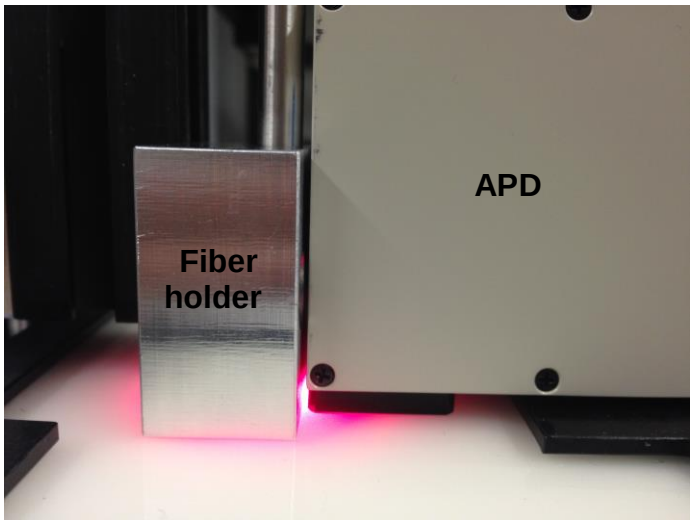

Figure 7. Source-detector configuration in reflectance mode.

The electrical output of the APD is high-pass filtered at 41 MHz and routed to one channel of the 2-channel ADC (Table 3), while the combined reference signal from the power combiner is routed to the other channel of the ADC. At each frequency step, the ADC typically collects 4096 samples on each channel of the ADC. If the user wishes to lower the noise floor, more samples can be collected (i.e. 8192, 16,384…2^n), but increasing the number of samples per step substantially increases data transfer and processing time. Both channels of the ADC run off of the same clock, which allows them to sample simultaneously with a high level of precision. Each channel samples at 250 MSPS.

ADC Specifications	
Bit-depth	14 bit
Full scale input voltage	2 V_{pp}
Max sampling rate	250 MSPS
Power consumption	1.25 W

Table 3. Analog to digital converter (ADC) specifications

Signal Processing

All signal processing is performed in Matlab (R2014b, Mathworks Natick, MA). The two-channel ADC samples at 250 MSPS, which, for the up to 400 MHz modulation frequencies used in the dDOSI system, is less than the Nyquist criterion requiring a sampling rate of at least twice the bandwidth of the signal of interest to avoid aliasing. All signals modulated above 125 MHz are aliased; however, given that the exact modulation frequency is known for each wavelength at each frequency step, the signal of interest can be located in the baseband, as shown in Figure 8. The processing algorithm eliminates modulation

frequencies that are multiples of the Nyquist frequency, then maps all measured (aliased) frequencies in the baseband to the corresponding original modulation frequencies, and removes any frequency steps at which the modulation frequencies for multiple wavelengths are aliased to the same frequency in the baseband (i.e. with a Nyquist frequency of 125 MHz, signals at 120 and 130 MHz would both be read as 120 MHz, and thus both frequency steps would be eliminated from processing).

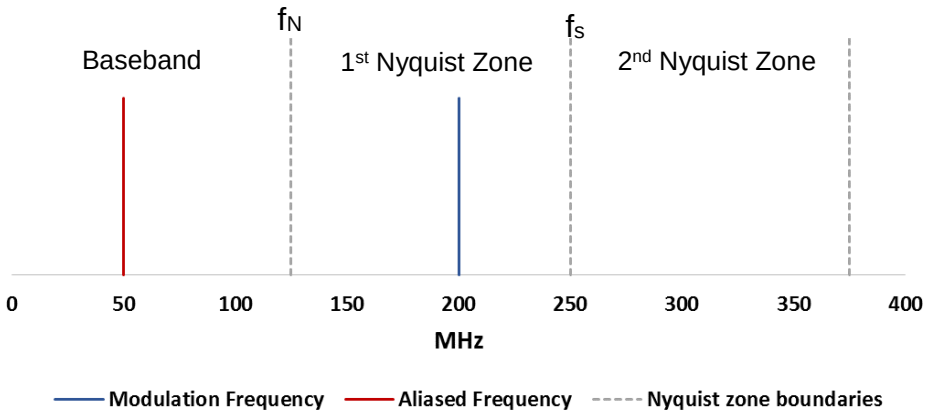

Figure 8. Example of undersampling signal detection. With a modulation frequency of 200 MHz and a sampling rate of 250 MSPS, the signal of interest is aliased at 50 MHz. fs, sampling frequency; fN, Nyquist frequency.

A fast Fourier transform (FFT) with a rectangular window is performed at each frequency step for the reference and measurement channels. The appropriate frequency bin is located for each wavelength at each modulation frequency step. The magnitude of the FFT of the measurement channel relative to that of the reference channel is considered the raw amplitude value, and, similarly, the phase offset between the measurement and reference channels is considered the raw phase value.

Measurement Calibration

The raw amplitude and phase reflect the amplitude attenuation and phase delay induced both by the tissue and by the instrument itself. In order to remove the instrument response, a measurement is taken on a silicone phantom with known optical properties. An analytical solution to the P1 approximation of the Boltzman Transport Equation with boundary conditions for semi-infinite geometry[17] is employed to calculate the forward model for the phantom measurement, which provides the theoretical amplitude attenuation and phase shift for the given optical properties and source-detector separation at each modulation frequency. Calibration factors for amplitude and phase are determined by ratiometrically or differentially comparing the measured amplitude and phase, respectively, to the theoretical amplitude and phase from the forward model. These calibration factors are then applied to the raw amplitude and phase measurements in order to obtain calibrated amplitude and phase, which consider only the effect of the tissue. A Matlab script developed by Prof. Bruce Tromberg's research group at the Beckman Laser Institute is used for all measurement calibration, optical property recovery, and chromophore concentration calculation.

Optical Property and Chromophore Recovery

The calibrated amplitude and phase measurements are used in an inverse model to approximate absorption (μ_a) and scattering (μ_s') parameters at each

wavelength. μ_a and μ_s' are input into an analytical solution to the P1 diffusion approximation of Boltzman Transport Equation, then least-squares fitting is employed to minimize the error between the back-calculated and measured calibrated amplitude and phase[17].

Chromophore extinction coefficients are obtained from Zijlstra *et al* [21]. A modified version of Beer's Law[20] (Equation 12) is used to relate μ_a to chromophore concentrations. A system of linear equations is used to calculate individual chromophore concentrations, such that there must be at least as many wavelengths employed as chromophores calculated.

User Interface

A custom graphical user interface (GUI), shown in Figure 9, designed in Matlab allows the user to set the desired parameters for frequency sweeps, data acquisition, and file storage. A typical clinical measurement requires the user to manually scan the source-detector pair across the tissue of interest in a grid pattern in order to create maps of tissue chromophore concentrations.

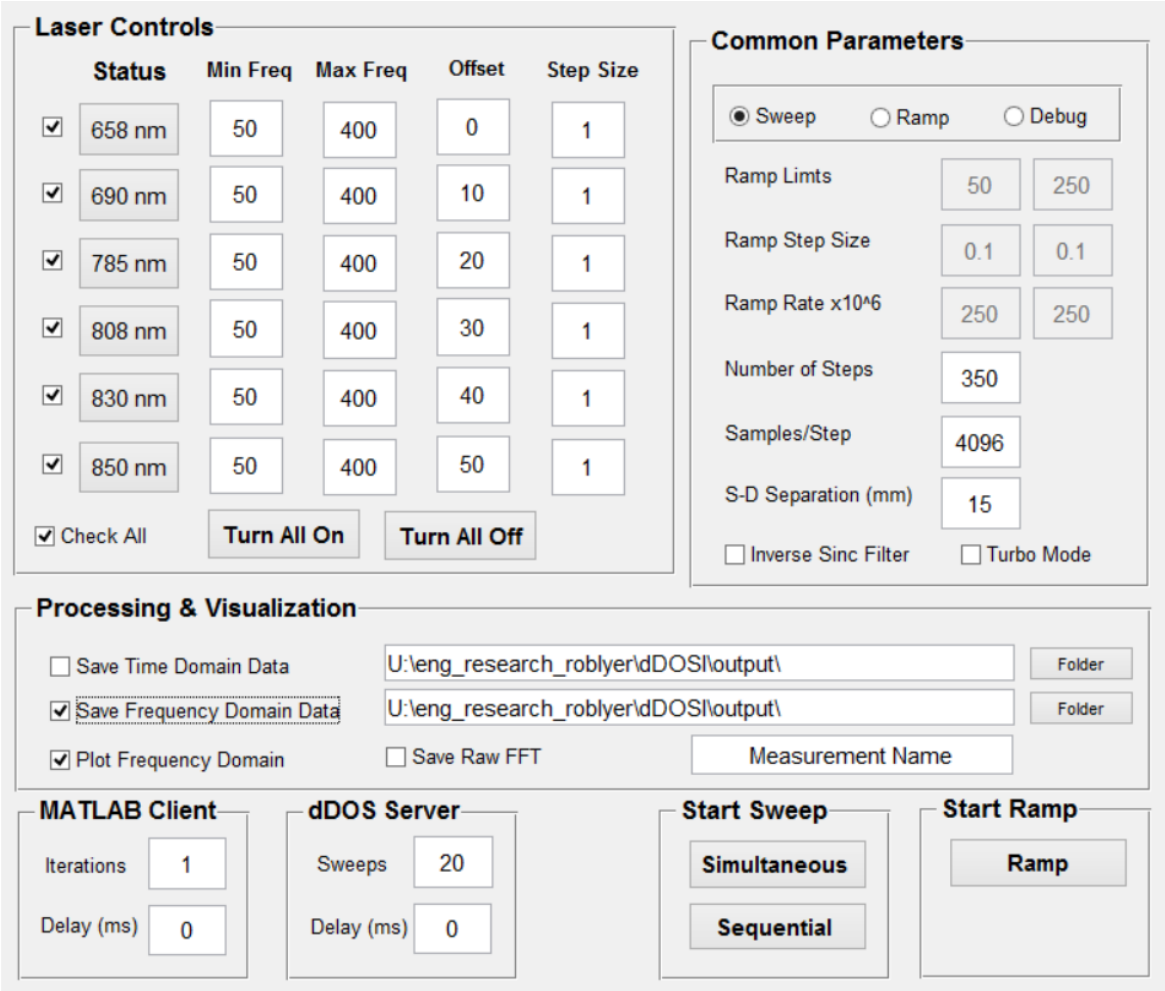

Figure 9. Graphical user interface for dDOSI system

Aim 2 Results: System Characterization

Signal to Noise

Signal to noise was determined by taking an FFT during a single frequency step with all six laser wavelengths employed simultaneously and with a single laser wavelength modulated individually. Frequency steps of both 4096 and 8192 samples per step were analyzed and the noise floor was calculated as

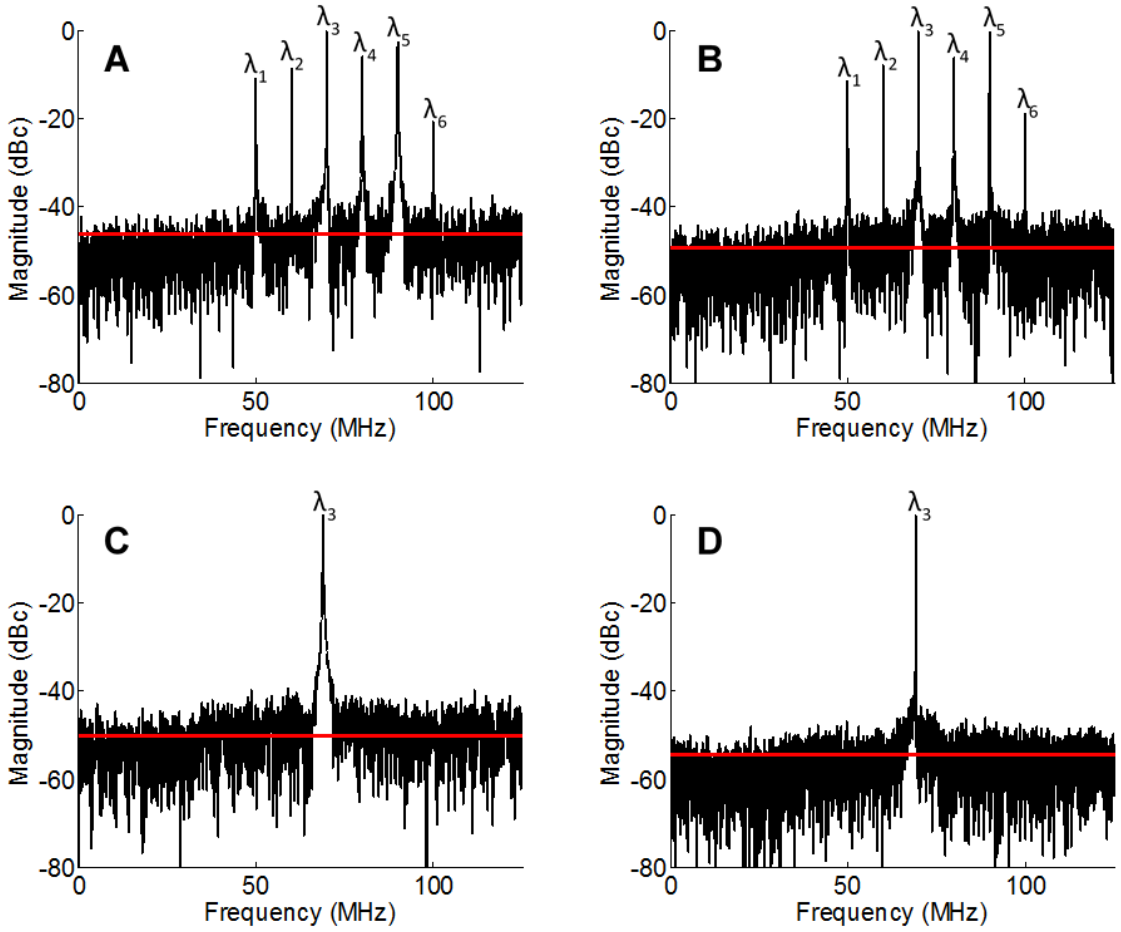

Figure 10. Signal to noise ratio. A. 6 wavelengths modulated simultaneously with 4096 samples acquired per frequency step. Noise floor = 46.29 dBc. B. 6 wavelengths modulated simultaneously with 8192 samples acquired per frequency step. Noise floor = 49.23 dBc. C. 785 nm laser modulated individually at 70 MHz with 4096 samples acquired per frequency step. Noise floor = 50.15 dBc. D. 785 nm laser modulated individually at 70 MHz with 8192 samples acquired per frequency step. Noise floor = 54.48 dBc.

the noise level, in dBc, relative to the laser with the greatest amplitude in the frequency domain, as shown in Figure 10. In the simultaneous measurement (Figure 10 A, B), the noise floor is reduced from -46.29 dBc to -49.23 dBc when increasing the number of samples per frequency step from 4096 to 8192. Similarly, in the single wavelength measurement (Figure 10 C, D), the noise floor is reduced from -50.15 dBc to -54.48 dBc when increasing the number of samples per frequency step from 4096 to 8192. Although the noise floor is lower with 8192, or more, samples per frequency step, acquisition time of such measurements was substantially slower than of those with 4096 samples per frequency step, and there was no improvement in accuracy of optical properties (accuracy of 10 measurements on 2 phantoms with 4096 samples per frequency step: 1.29%; accuracy with 8192 samples per frequency step: 1.85%); therefore, the primary measurement mode used 4096 samples per frequency step to optimize speed and accuracy.

Amplitude and Phase Measurements

Amplitude and phase were measured on a series of silicone phantoms using the dDOSI system with frequency sweeps from 50 to 400 MHz in steps of 1 MHz. An example of calibrated (black) and fit (red) amplitude and phase at each wavelength is shown in Figure 11. Data were calibrated using silicone phantoms with known optical properties in order to remove the instrument response. The

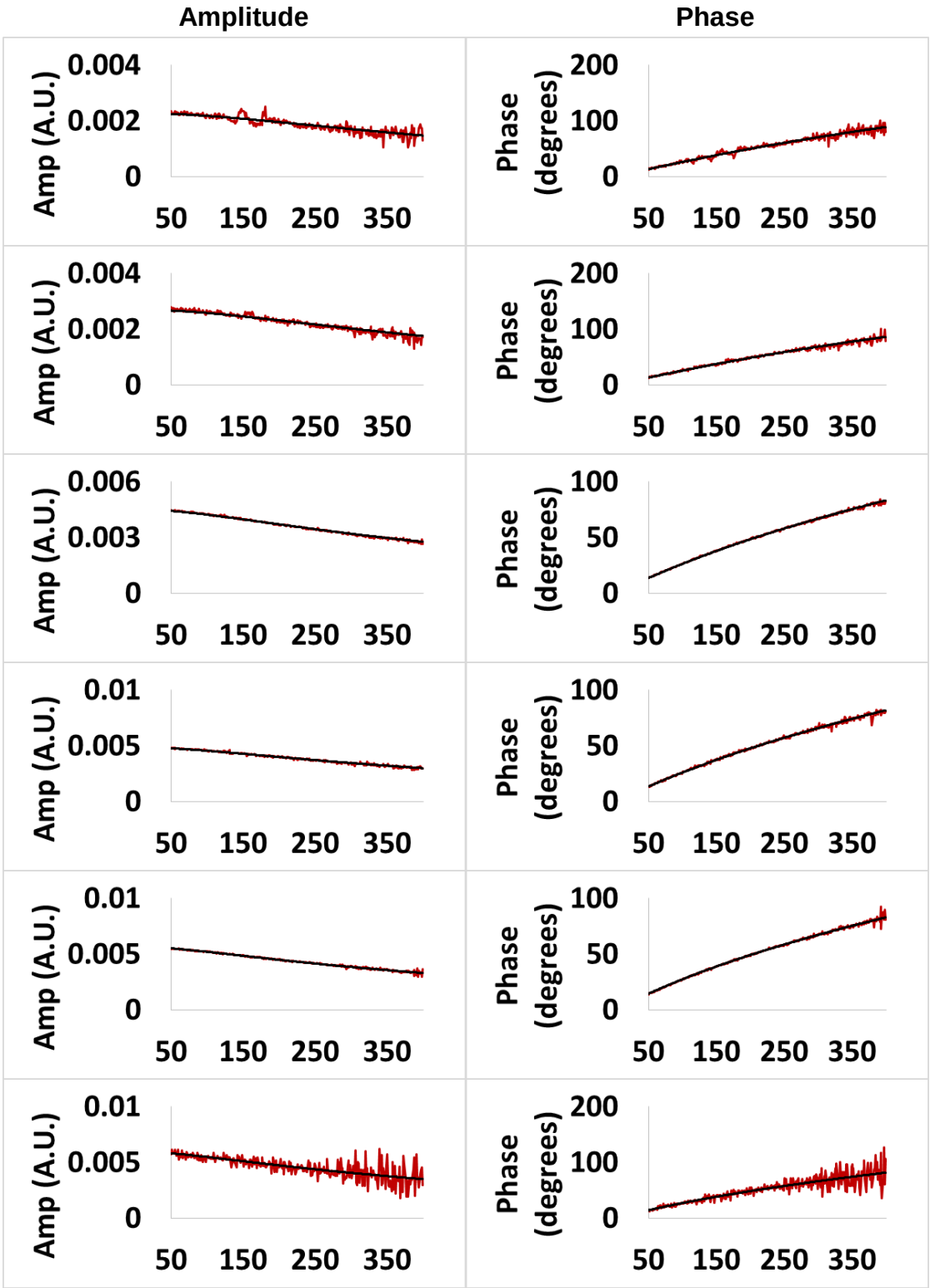

Figure 11. Amplitude (in arbitrary units, A.U.) and phase measured with dDOSI system at each wavelength. Red lines are calibrated data and black lines are model fits.

calibrated data were then fit using least-squares minimization for the P1 diffusion approximation of the Boltzman Transport Equation.

Figure 12 shows an example of calibrated data (black) and fit data (red) for both the fully miniaturized dDOSI system (i.e. fiber-coupled laser diode modules and portable current controller modules) and the benchtop DOSI system at 658 nm. For this example, amplitude and phase were compared for frequency sweeps from 50 to 400 MHz at 658 nm using both the benchtop DOSI system and the fully miniaturized dDOSI system. The dDOSI frequency sweep used 7 MHz steps, while the benchtop system used approximately 1 MHz steps. Data were calibrated using silicone phantoms with known optical properties in order to remove the instrument response. The calibrated data were then fit using least-squares minimization for the P1 diffusion approximation of Boltzman Transport Equation.

The fully miniaturized system performed well in initial testing, however the laser diode modules used were easily overdriven, possibly due to transient current spikes from the current controller modules or extreme sensitivity of the laser diodes. Additional safety components will be added to the current controller module PCB, and further testing will be performed to ensure that the fully miniaturized system is robust enough for clinical use.

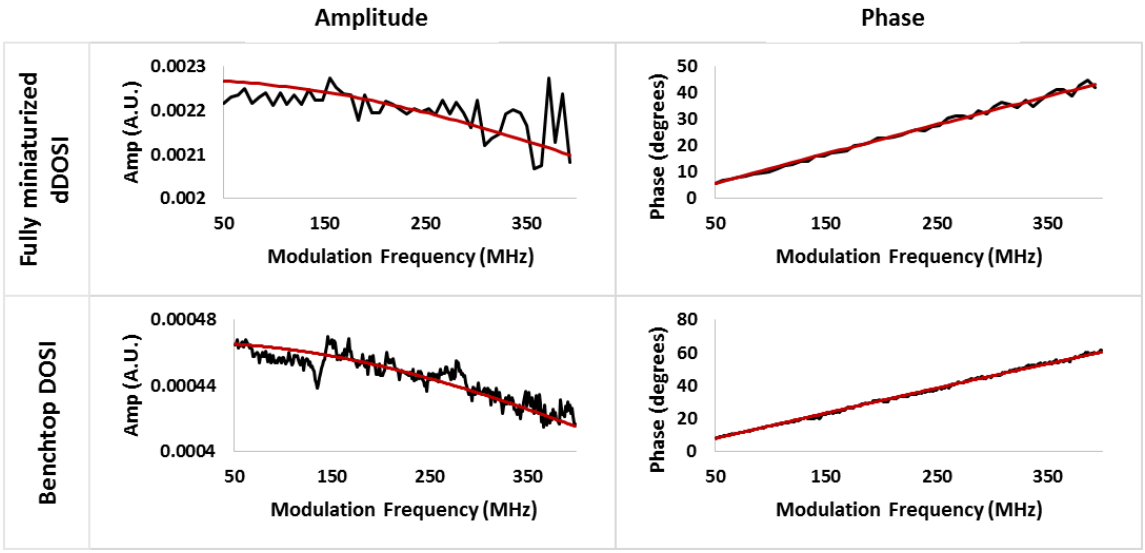

Figure 12. Amplitude (in arbitrary units, A.U.) and phase measured with fully miniaturized dDOSI system compared with benchtop system at 658 nm with 15 mm source-detector separation. Black lines represent calibrated data (i.e. instrument response removed) and red lines represent fits to the P1 diffusion approximation of the Boltzman Transport Equation.

Accuracy of Optical Properties

Optical properties were measured for 10 silicone phantoms with varying amounts of titanium dioxide and nigrosin, as the scattering and absorbing agents, respectively, using both the dDOSI and benchtop DOSI systems. For each phantom, 10 frequency domain measurements were taken with each system with a 15 mm source-detector separation and all six wavelengths modulated at frequencies between 50 and 400 MHz with 1 MHz frequency steps. 4096 samples were collected at each frequency step for the dDOSI system. Table 4 summarizes the mean optical properties measured with each system for each wavelength, showing the percent difference in optical properties between systems. For phantom #10 measurements at 658, 690, and 850 nm were

excluded due to phase errors resulting from low detected signal levels. The mean of the absolute difference in optical properties for all measured phantoms between the two systems was 5.3% and 5.5% for μ_a and μ_s', respectively; when frequency sweeps from 50-300 MHz were used, the mean accuracy in optical properties measured with the two systems was 4.9% and 6.0% for μ_a and μ_s', respectively.

phantom	wavelength (nm)	μ_a (mm^{-1})		μ_s' (mm^{-1})		% difference	
		dDOSI	benchtop	dDOSI	benchtop	μ_a	μ_s'
1	658	0.022 ± 0.0006	0.023 ± 0.0004	0.580 ± 0.010	0.627 ± 0.010	-3.6	-7.5
	690	0.019 ± 0.0004	0.020 ± 0.0011	0.584 ± 0.007	0.636 ± 0.025	-3.2	-8.2
	785	0.012 ± 0.0001	0.013 ± 0.0001	0.534 ± 0.003	0.588 ± 0.004	-6.9	-9.2
	808	0.011 ± 0.0001	0.011 ± 0.00005	0.510 ± 0.004	0.561 ± 0.002	-6.0	-9.2
	830	0.010 ± 0.0001	0.011 ± 0.00003	0.480 ± 0.002	0.544 ± 0.003	-6.3	-11.7
	850	0.010 ± 0.0004	0.010 ± 0.00005	0.479 ± 0.014	0.539 ± 0.001	-5.2	-11.1
2	658	0.021 ± 0.0007	0.021 ± 0.0003	0.611 ± 0.014	0.653 ± 0.006	-1.2	-6.5
	690	0.018 ± 0.0002	0.019 ± 0.0007	0.616 ± 0.007	0.645 ± 0.018	-4.5	-4.5
	785	0.010 ± 0.0001	0.011 ± 0.0001	0.569 ± 0.003	0.619 ± 0.003	-6.6	-8.1
	808	0.009 ± 0.0001	0.009 ± 0.0002	0.554 ± 0.003	0.600 ± 0.010	-4.5	-7.7
	830	0.008 ± 0.0001	0.009 ± 0.00005	0.530 ± 0.002	0.584 ± 0.002	-6.6	-9.2
	850	0.007 ± 0.0003	0.008 ± 0.00005	0.530 ± 0.011	0.581 ± 0.001	-6.5	-8.7
3	658	0.021 ± 0.0006	0.022 ± 0.0003	0.904 ± 0.014	0.942 ± 0.010	-6.6	-4.0
	690	0.018 ± 0.0005	0.019 ± 0.0003	0.891 ± 0.013	0.922 ± 0.009	-6.2	-3.4
	785	0.010 ± 0.0001	0.011 ± 0.0001	0.820 ± 0.002	0.882 ± 0.002	-8.0	-7.0
	808	0.009 ± 0.0001	0.010 ± 0.0001	0.798 ± 0.006	0.859 ± 0.003	-7.3	-7.0
	830	0.008 ± 0.00004	0.009 ± 0.00002	0.776 ± 0.001	0.848 ± 0.002	-9.2	-8.5
	850	0.007 ± 0.0004	0.008 ± 0.00004	0.772 ± 0.020	0.844 ± 0.001	-8.8	-8.6
4	658	0.004 ± 0.0001	0.004 ± 0.0001	1.348 ± 0.007	1.358 ± 0.004	1.1	-0.7
	690	0.004 ± 0.0001	0.004 ± 0.00004	1.288 ± 0.007	1.285 ± 0.005	-1.8	0.3
	785	0.002 ± 0.00001	0.002 ± 0.00002	1.096 ± 0.001	1.110 ± 0.003	0.2	-1.3
	808	0.002 ± 0.00003	0.002 ± 0.0001	1.052 ± 0.004	1.062 ± 0.003	9.4	-0.9
	830	0.001 ± 0.00001	0.001 ± 0.00001	1.021 ± 0.001	1.036 ± 0.003	1.9	-1.4
	850	0.001 ± 0.0001	0.001 ± 0.00003	1.008 ± 0.009	1.023 ± 0.001	0.2	-1.5
5	658	0.017 ± 0.0005	0.017 ± 0.0002	0.717 ± 0.012	0.726 ± 0.005	1.3	-1.2
	690	0.014 ± 0.0003	0.015 ± 0.0003	0.706 ± 0.008	0.700 ± 0.011	-1.8	0.8
	785	0.007 ± 0.0001	0.008 ± 0.00005	0.634 ± 0.002	0.649 ± 0.002	-2.8	-2.3
	808	0.006 ± 0.0001	0.006 ± 0.0001	0.614 ± 0.005	0.616 ± 0.003	2.3	-0.3
	830	0.006 ± 0.00003	0.006 ± 0.00003	0.586 ± 0.001	0.601 ± 0.002	2.2	-2.6
	850	0.005 ± 0.0002	0.005 ± 0.00005	0.582 ± 0.009	0.594 ± 0.001	2.2	-1.9
6	658	0.043 ± 0.0023	0.047 ± 0.0003	0.582 ± 0.031	0.594 ± 0.003	-8.8	-1.9
	690	0.040 ± 0.0005	0.041 ± 0.0019	0.550 ± 0.007	0.601 ± 0.028	-1.4	-8.4
	785	0.024 ± 0.0002	0.025 ± 0.0002	0.511 ± 0.003	0.557 ± 0.003	-5.0	-8.4
	808	0.021 ± 0.0003	0.022 ± 0.0002	0.503 ± 0.007	0.544 ± 0.005	-5.8	-7.5
	830	0.021 ± 0.0001	0.021 ± 0.0001	0.455 ± 0.002	0.512 ± 0.002	-3.5	-11.3
	850	0.019 ± 0.0008	0.020 ± 0.0001	0.455 ± 0.017	0.519 ± 0.001	-3.1	-12.4
7	658	0.050 ± 0.0024	0.053 ± 0.0027	0.399 ± 0.025	0.424 ± 0.028	-5.9	-5.8
	690	0.042 ± 0.0013	0.044 ± 0.0036	0.419 ± 0.014	0.453 ± 0.044	-4.2	-7.6
	785	0.024 ± 0.0003	0.026 ± 0.0001	0.411 ± 0.006	0.452 ± 0.002	-7.3	-9.1
	808	0.021 ± 0.0006	0.023 ± 0.0001	0.407 ± 0.011	0.442 ± 0.003	-8.3	-8.0
	830	0.020 ± 0.0002	0.022 ± 0.0001	0.367 ± 0.004	0.418 ± 0.004	-7.1	-12.2
	850	0.017 ± 0.0043	0.020 ± 0.0001	0.309 ± 0.128	0.425 ± 0.001	-16.0	-27.5
8	658	0.009 ± 0.0001	0.009 ± 0.0001	0.874 ± 0.006	0.871 ± 0.006	-1.1	0.3
	690	0.010 ± 0.0002	0.010 ± 0.0003	0.859 ± 0.011	0.857 ± 0.013	-1.0	0.3
	785	0.008 ± 0.00005	0.008 ± 0.0001	0.815 ± 0.002	0.814 ± 0.002	-0.5	0.2
	808	0.006 ± 0.0002	0.006 ± 0.0002	0.836 ± 0.009	0.834 ± 0.009	-1.0	0.3
	830	0.004 ± 0.00001	0.004 ± 0.00002	0.831 ± 0.001	0.829 ± 0.001	-1.2	0.2
	850	0.004 ± 0.00005	0.004 ± 0.00005	0.827 ± 0.002	0.824 ± 0.002	-1.5	0.4
9	658	0.003 ± 0.0001	0.003 ± 0.0001	1.375 ± 0.005	1.418 ± 0.012	-6.8	-3.1
	690	0.002 ± 0.00004	0.003 ± 0.0001	1.286 ± 0.006	1.327 ± 0.012	-9.5	-3.1
	785	0.001 ± 0.00002	0.002 ± 0.00004	1.079 ± 0.003	1.120 ± 0.003	-18.5	-3.7
	808	0.001 ± 0.00003	0.001 ± 0.0001	1.054 ± 0.004	1.089 ± 0.005	-15.9	-3.2
	830	0.001 ± 0.00003	0.001 ± 0.00002	1.006 ± 0.002	1.039 ± 0.004	-16.1	-3.2
	850	0.001 ± 0.0002	0.001 ± 0.00002	0.975 ± 0.023	1.027 ± 0.001	5.8	-5.0
10	785	0.034 ± 0.0001	0.034 ± 0.0002	0.891 ± 0.003	0.891 ± 0.004	0.9	0.0
	808	0.033 ± 0.0006	0.032 ± 0.0004	0.854 ± 0.014	0.864 ± 0.009	2.2	-1.2
	830	0.028 ± 0.0002	0.027 ± 0.0001	0.834 ± 0.005	0.833 ± 0.003	0.7	0.0

Table 4. Optical properties measured with dDOSI and benchtop DOSI systems. Optical property values are mean ± standard deviation for 10 measurements.

Figures 13 and 14 show Bland-Altman[33] plots for μ_a and μ_s' measured with the dDOSI and benchtop DOSI systems, where the differences between optical properties with the dDOSI and benchtop system are plotted on the y-axis versus average optical properties for each system on the x-axis, for each wavelength and phantom. Nearly all values fall within 1.96 standard deviations of the mean difference, indicating acceptable precision between the two systems. μ_a and μ_s' both tend to skew slightly lower for the dDOSI system compared to the benchtop DOSI system. Figures 15 and 16 show scatterplots of optical properties measured with each system. μ_a values had the best agreement between systems when the mean absorption coefficient was less than .015 mm^{-1}, while μ_s' had the best agreement between systems when the mean reduced scattering coefficient was greater than 1 mm^{-1}. In healthy breast tissue μ_a in the NIR is typically less than 0.01 mm^{-1}, and μ_s' in the NIR is typically greater than 0.8 mm^{-1} [34]; therefore, the dDOSI system is likely to be capable of extracting accurate optical properties in physiological range for breast tissue.

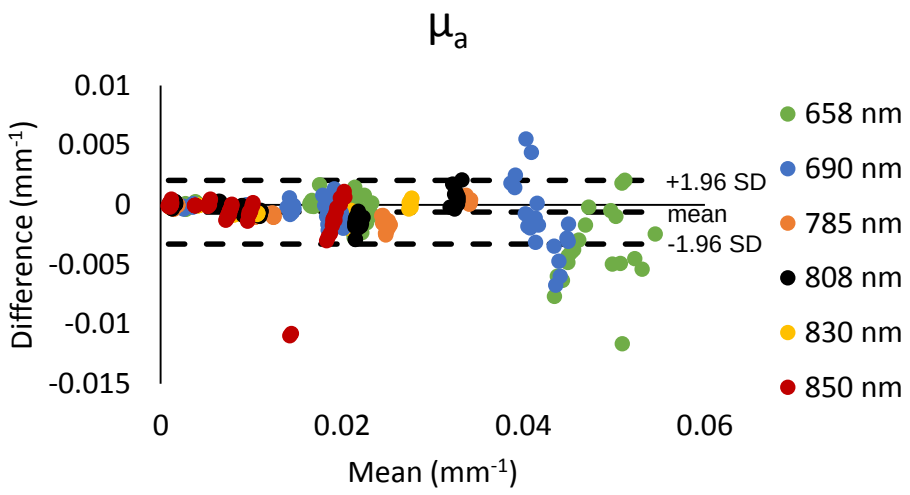

Figure 13. Bland-Altman plots showing the difference in μ_a measured by the dDOSI system and the benchtop DOSI system plotted against the mean for 10 measurements on each of 10 silicon phantoms with varying optical properties using the two systems. Top and bottom dashed lines represent 1.96 standard deviations from the mean difference (center dashed line).

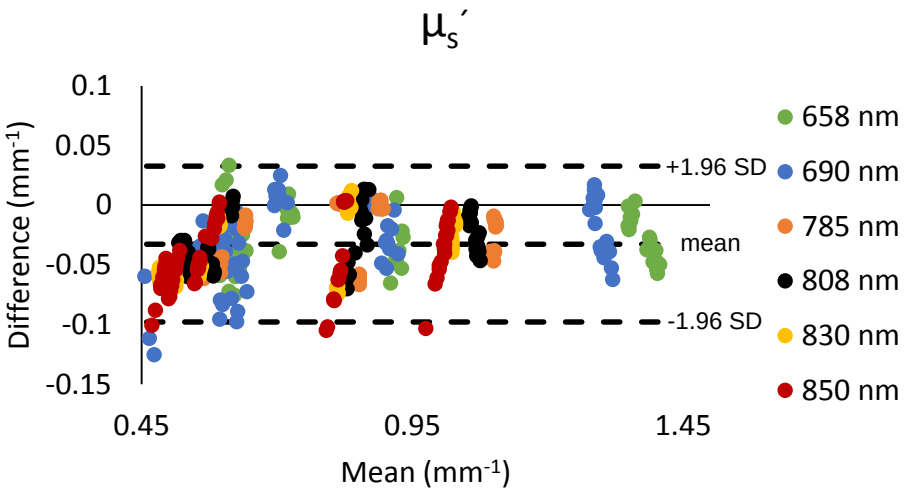

Figure 14. Bland-Altman plots showing the difference in μ_s' measured by the dDOSI system and the benchtop DOSI system plotted against the mean for 10 measurements on each of 10 silicon phantoms with varying optical properties using the two systems. Top and bottom dashed lines represent 1.96 standard deviations from the mean difference (center dashed line).

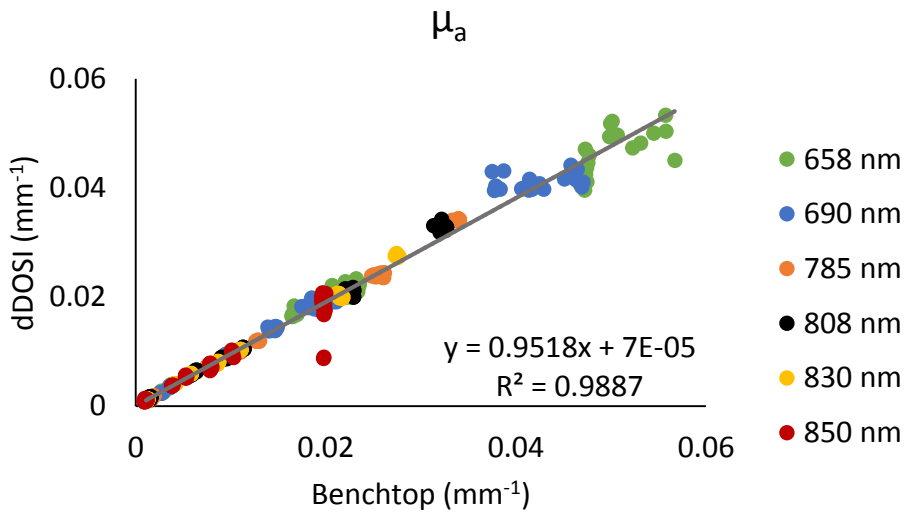

Figure 15. Scatterplot of μ_a measured with the dDOSI and benchtop systems, each utilizing modulation frequencies between 50 and 400 MHz with 1 MHz steps. 10 measurements were taken on each of 10 phantoms using each system. Gray line represent a linear fit, described by the given equation and R^2.

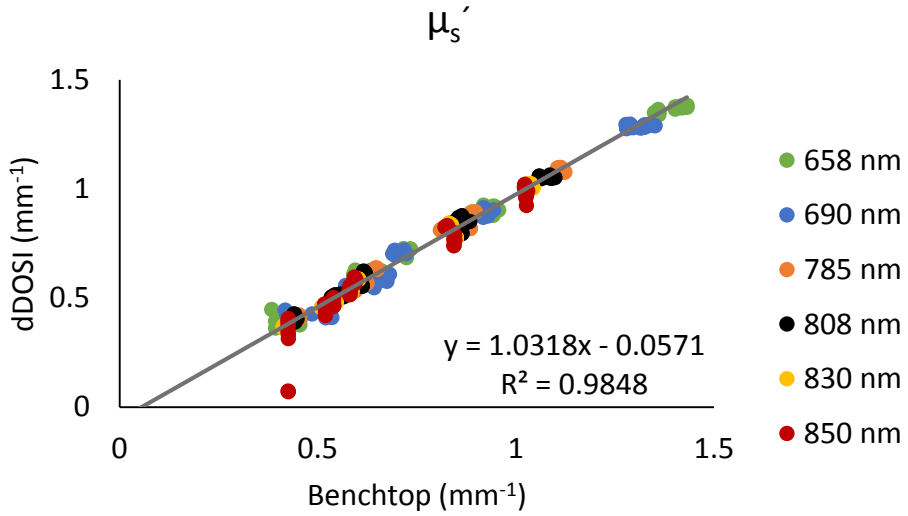

Figure 16. Scatterplot of $\mu_{s'}$ measured with the dDOSI and benchtop systems, each utilizing modulation frequencies between 50 and 400 MHz with 1 MHz steps. 10 measurements were taken on each of 10 phantoms using each system. Gray line represent a linear fit, described by the given equation and R^2.

The fully miniaturized dDOSI system, which includes compact fiber-coupled laser diode modules and portable current controller modules, underwent preliminary testing. Optical properties were measured for phantom #5 (Table 4) in a series of 5 measurements using the 658 nm laser diode modulated with a frequency sweep from 50-400 MHz with steps of 7 MHz and a 15 mm source-detector separation, then compared to optical properties measured with the benchtop DOSI system. Mean and standard deviation of measurements with each system are shown in Table 5.

	dDOSI	benchtop	% difference
μ_a (mm^{-1})	0.0178 ± 0.0002	0.018 ± 0.0001	-1.71
μ_s' (mm^{-1})	0.707 ± 0.006	0.737 ± 0.008	-4.14

Table 5. Optical properties at 658 nm using the fully miniaturized dDOSI system compared with the bencthtop DOSI system. 5 consecutive measurements were taken with each system. Optical property values are mean ± standard deviation.

Precision Validation

Neoadjuvant chemotherapy infusions in the protocol used by our group at Boston Medical Center typically last approximately two hours, and the dDOSI system will be used to take measurements at various time points throughout an infusion. Thus, the stability of amplitude, phase, and optical properties have been characterized during a two hour drift test. Measurements were taken at approximately one minute intervals on a silicone optical phantom (phantom #5, Table 4) using 690, 785, 808, 830, and 850 nm lasers modulated simultaneously in frequency sweeps from 50-400 MHz with a 15 mm source-detector separation.

Amplitude and phase were examined for the duration of the drift test for the 808 nm laser modulated at 50 MHz and were plotted in Figures 17 and 18. For this wavelength and modulation frequency, phase drift had a standard deviation of 0.54 degrees and amplitude drift had a standard deviation of 0.89%.

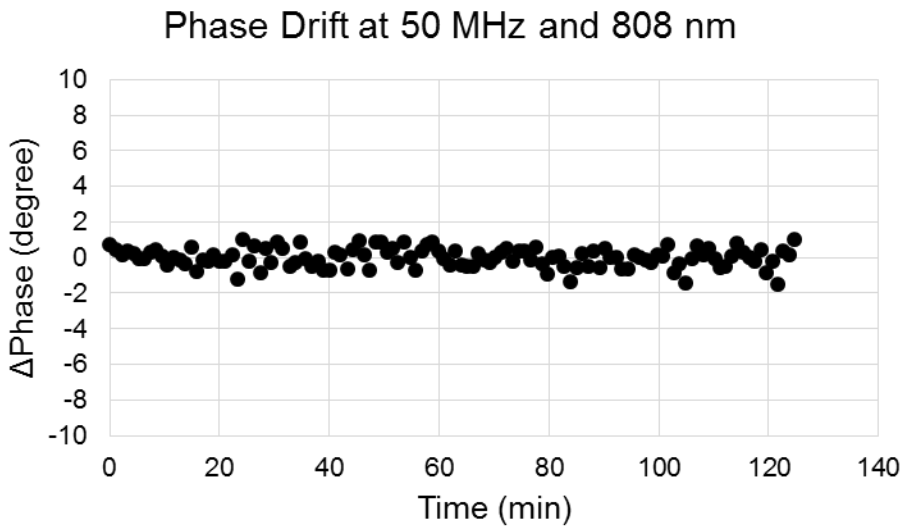

Figure 17. Phase measurements for 808 nm laser diode modulated at 50 MHz during a two hour drift test with measurements taken approximately every minute.

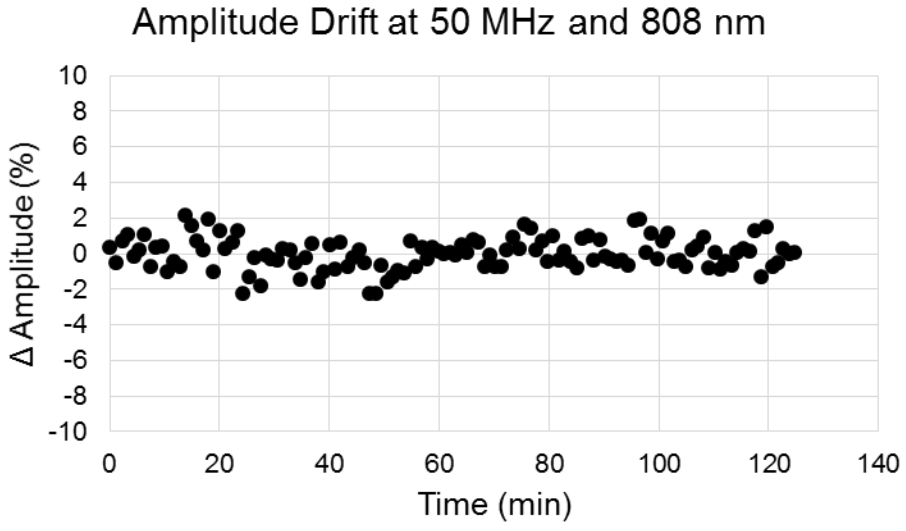

Figure 18. Amplitude measurements for 808 nm laser diode modulated at 50 MHz during a two hour drift test with measurements taken approximately every minute.

System stability was further analyzed for all wavelengths and modulation frequencies used in the drift test, as shown in Table 6. Amplitude and optical property stability were defined as the standard deviation divided by the mean at each modulation frequency, averaged for all wavelengths. Phase stability was defined as the standard deviation throughout the drift test averaged for all wavelengths and modulation frequencies. Although there was somewhat increased variability in amplitude and phase when examining all wavelengths and modulation frequencies, rather than a single wavelength and modulation frequency, the stability in μ_a and μ_s' was 2.65% and 1.34%, respectively, throughout the drift test. The good stability in optical properties was likely influenced by the large range of modulation frequencies used to fit the diffusion model.

Average stability across all wavelengths and modulation frequencies	
amplitude	2.7%
phase	3.8˚
μ_a	2.6%
μ_s'	1.3%

Table 6. System stability during 2-hour drift test.

Speed

Previous frequency domain DOSI instruments[17], [32] have performed frequency sweeps with each wavelength modulated individually in a sequential manner. The dDOSI system, however, utilizes wavelength multiplexing, which eliminates switching time between lasers and reduces data acquisition time,

resulting in the ability to measure fast physiological changes. The rate at which frequency sweep measurements can be performed is dependent on the range of modulation frequencies and the number of discrete steps used. Table 7 shows the rate at which physiological changes can be detected, using various frequency ranges and step sizes. The maximum speed achieved with frequency sweep (50-300 MHz) measurements with the dDOSI system was 97.2 Hz, which is fast enough to detect physiological changes at the cardiac rate with good temporal resolution.

Frequency Sweep Measurement Speeds			
Range	Step size	Measurement time (ms)	Measurement rate (Hz)
50 - 300 MHz	1 MHz	71.9	13.9
	7 MHz	10.3	97.2
50 - 400 MHz	1 MHz	102	9.78
	7 MHz	14.7	68.1

Table 7. Frequency sweep measurement rates.

In order to test the maximum measurement speed attainable with the dDOSI system, measurements were also taken with a single modulation frequency. When modulating at only 50 MHz, a measurement rate of 2557 Hz can be achieved. Although this is not the preferred data acquisition mode, because utilizing additional modulation frequencies improves model fit accuracy, it provides a useful comparison to other frequency domain systems which utilize a single modulation frequency[22]–[27].

Aim 3 Results: *In vivo* Testing

Cuff Occlusion Measurement

In vivo testing was performed in order to verify that acquired optical properties yielded physiologically appropriate chromophore values. The first *in vivo* measurement was a cuff occlusion in which a blood pressure cuff was placed on the upper arm and optical measurements were taken on the forearm of a 27-year-old female volunteer. The cuff was loosely secured in order to measure baseline levels of oxy- and deoxyhemoglobin then was inflated to 260 mmHg for approximately 3 minutes. The cuff was released and data were acquired for approximately 3 additional minutes. Frequency sweeps between 50 and 400 MHz, with frequency steps of 7 MHz, were used to modulate all 6 laser diodes simultaneously. Measurements were taken approximately every 4 seconds for 7 minutes. Source-detector separation was set to 15 mm, and in vivo measurements were calibrated using a silicone phantom with known optical properties. Chromophore concentrations were calculated for oxy, deoxy- and total hemoglobin for each measurement.

Figure 19 shows oxy- and deoxyhemoglobin concentrations throughout the cuff occlusion test. At baseline average oxy- and deoxyhemoglobin concentrations were 46.6 and 29.7 μM, respectively. At the time of cuff release, oxyhemoglobin concentration had dropped to 33.6 μM and deoxyhemoglobin had increased to 40.1 μM. After cuff release oxyhemoglobin rebounded to a local maximum of 63.0 μM and deoxyhemoglobin dropped to 18.6 μM, before both

chromophore concentrations began to return toward their baseline values. These results are consistent with arterial flow reduction during cuff occlusion, followed by a rush of arterial blood into the forearm after cuff release.

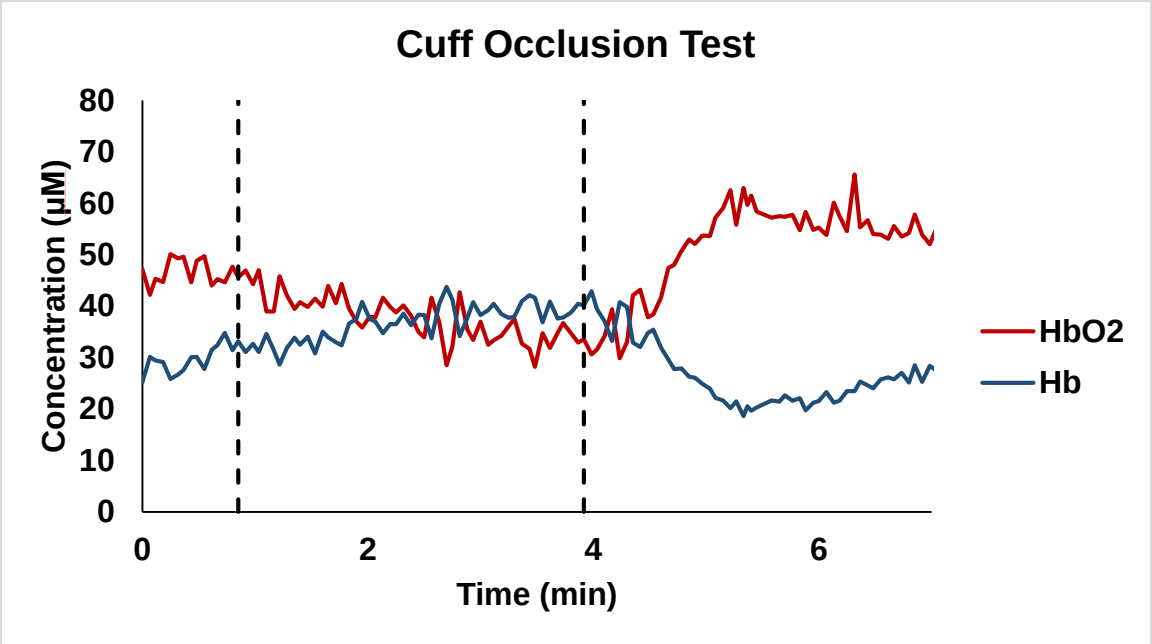

Figure 19. Forearm cuff occlusion test. Cuff was occluded during time interval between dashed lines.

Rapid *in vivo* Measurements

In order to test the ability of the dDOSI system to measure physiological changes at the cardiac rate, frequency sweep measurements were taken on the finger of a 27-year-old female volunteer. Measurements were taken in transmission mode at the base of the finger with a 15 mm source-detector separation. Frequency sweeps from 50-300 MHz with 7 MHz steps were used to modulate all 6 laser diodes simultaneously. 350 frequency sweeps were measured with a measurement rate of 97.1 Hz. A silicone phantom with known

optical properties was used to calibrate amplitude and phase measurements. Chromophore concentrations were calculated using optical properties from the 690, 785, 808, and 830 nm laser diodes. The analytical solution to the P1 approximation of the Boltzman Transport Equation with semi-infinite boundary conditions was used to fit reflectance mode calibration phantom measurements, while that with infinite boundary conditions[17] was used to fit the transmission mode finger measurements.

An ECG signal was measured simultaneously with the optical signal. The dDOSI system was configured to output a digital sample at the beginning of each frequency sweep. The ECG signal and dDOSI digital signals were detected simultaneously on an external data acquisition board, such that the optical signal could be synchronized with the ECG signal. Figures 20-24 show 5-point moving averages of optical properties and chromophore concentrations from the finger transmission measurement temporally aligned with the ECG. In Figure 20, μ_a values fluctuate temporally with the cardiac cycle, likely due to increased blood volume in the figure after ventricular contraction. There is a lag in the upstroke of the μ_a signal after the R-wave of the ECG, given the transmission time to the peripheral vasculature, which typically ranges from about 200 to 300 ms from R-wave to the upstroke of the photoplethysmographic signal measured in the fingertip[35]. Figure 21 shows that there is substantially less variation in μ_s', compared with μ_a, throughout the cardiac cycle.

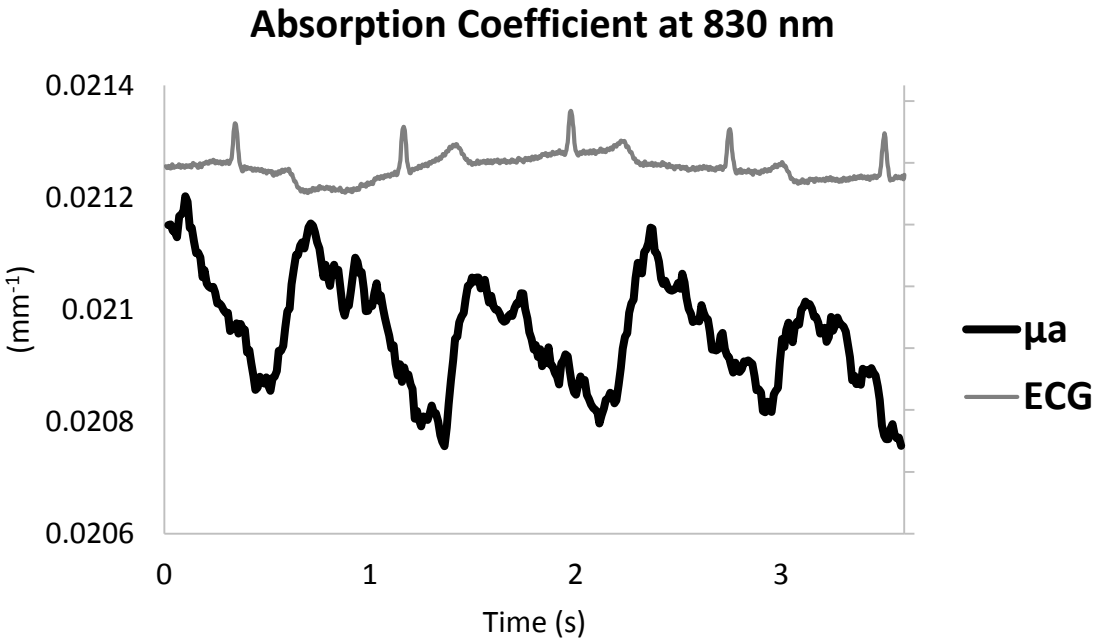

Figure 20. Absorption coefficient measured in the finger throughout the cardiac cycle and temporally aligned with an ECG.

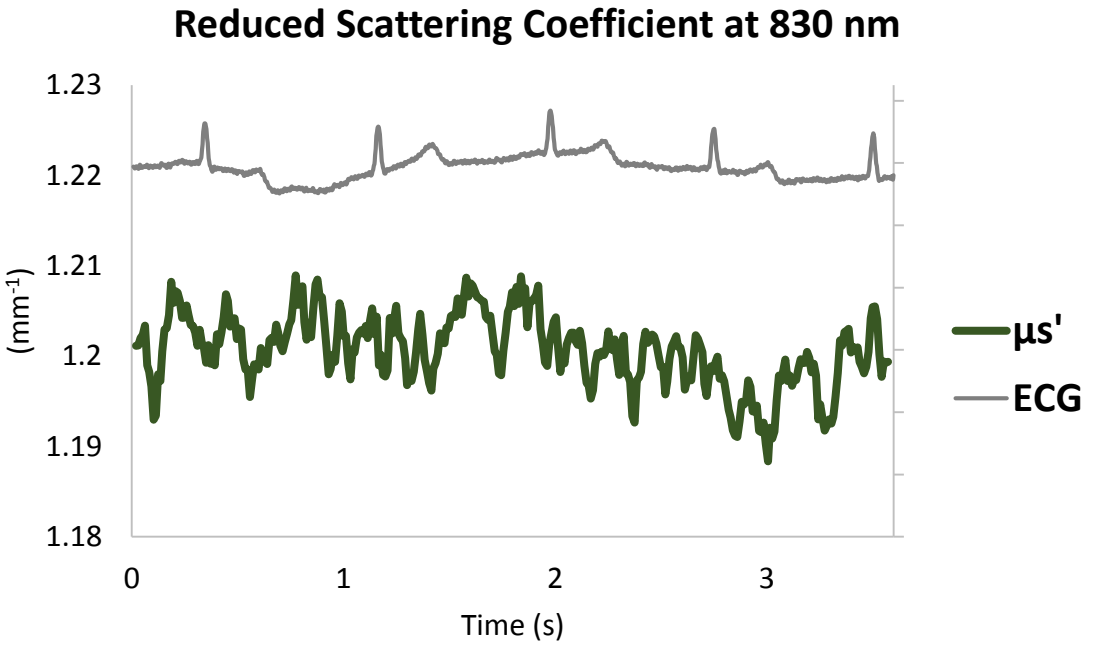

Figure 21. Reduced scattering coefficient measured in the finger throughout the cardiac cycle and temporally aligned with an ECG.

Chromophore values were measured throughout the cardiac cycle. Arterial blood is oxygen-rich and has a pulsatile flow profile, while venous blood contains less oxygen and the flow is more constant, as compared to arterial flow. Figure 22 shows that oxyhemoglobin concentration fluctuates at the same frequency as the ECG signal, suggesting that the dDOSI system is capable of detecting pulsatile, oxygenated, arterial blood flow. Figure 23 shows that deoxyhemoglobin concentration remains relatively constant throughout the cardiac cycle, given the lack of deoxyhemoglobin in the pulsatile arterial flow. Finally, total hemoglobin, shown in Figure 24, varies closely with the ECG signal, indicative of fluctuations in blood volume throughout the cardiac cycle.

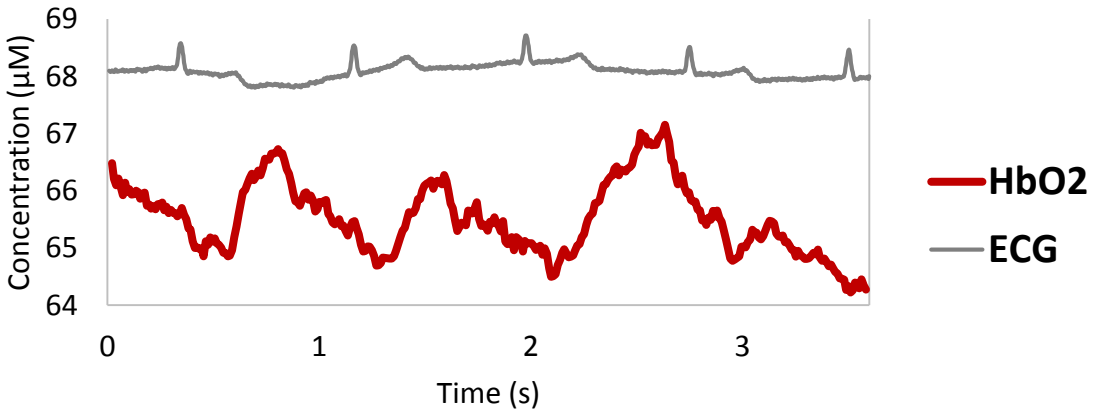

Figure 22. Oxyhemoglobin (HbO_2) concentration measured throughout the cardiac cycle.

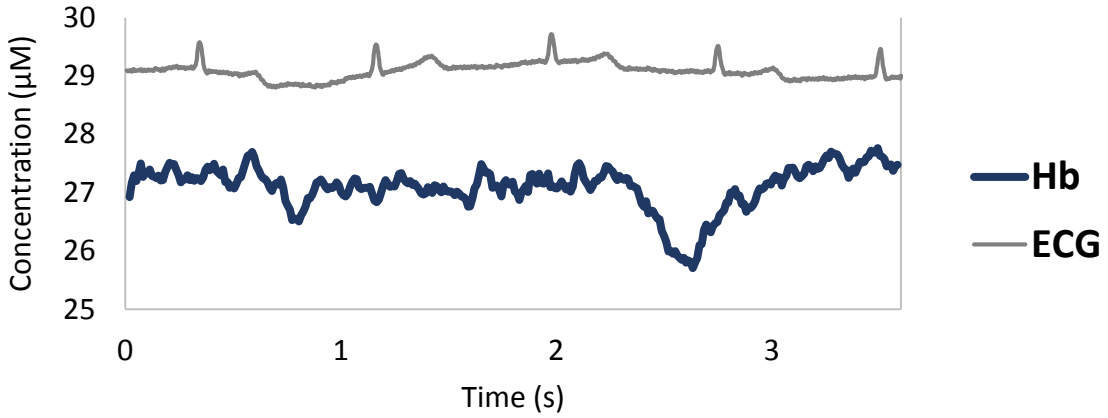

Figure 23. Deoxyhemoglobin (Hb) concentration measured throughout the cardiac cycle.

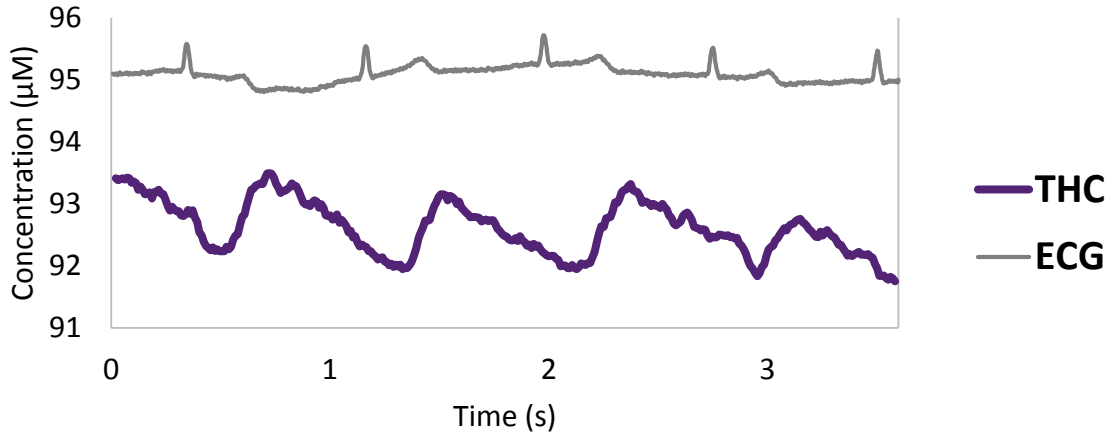

Figure 24. Total hemoglobin concentration (THC) measured throughout the cardiac cycle.

Chromophore Maps in Healthy Breast Tissue

Optical properties of breast tissue were measured on a healthy 28-year-old female volunteer. Measurements were taken with the dDOSI system using 658, 690, 785, 808, 830, and 850 nm lasers with a 28 mm source-detector

separation and modulation frequencies from 50 to 400 MHz. 36 point measurements were taken in which the source-detector pair was manually scanned across the right breast in a 6 x 6 grid pattern with 1 cm spacing between measurement points. A quadrant of the areolar complex was located at the bottom left corner of the imaging grid, covering approximately 2 cm vertically and 1 cm horizontally of the imaging area. Optical properties were calculated and chromophore values determined for each data point. Data from the 658 and 850 nm wavelengths were excluded due to noise in the phase measurement at these wavelengths. Figure 25 shows chromophore maps for deoxyhemoglobin and total hemoglobin concentrations with linear interpolation between measurement points.

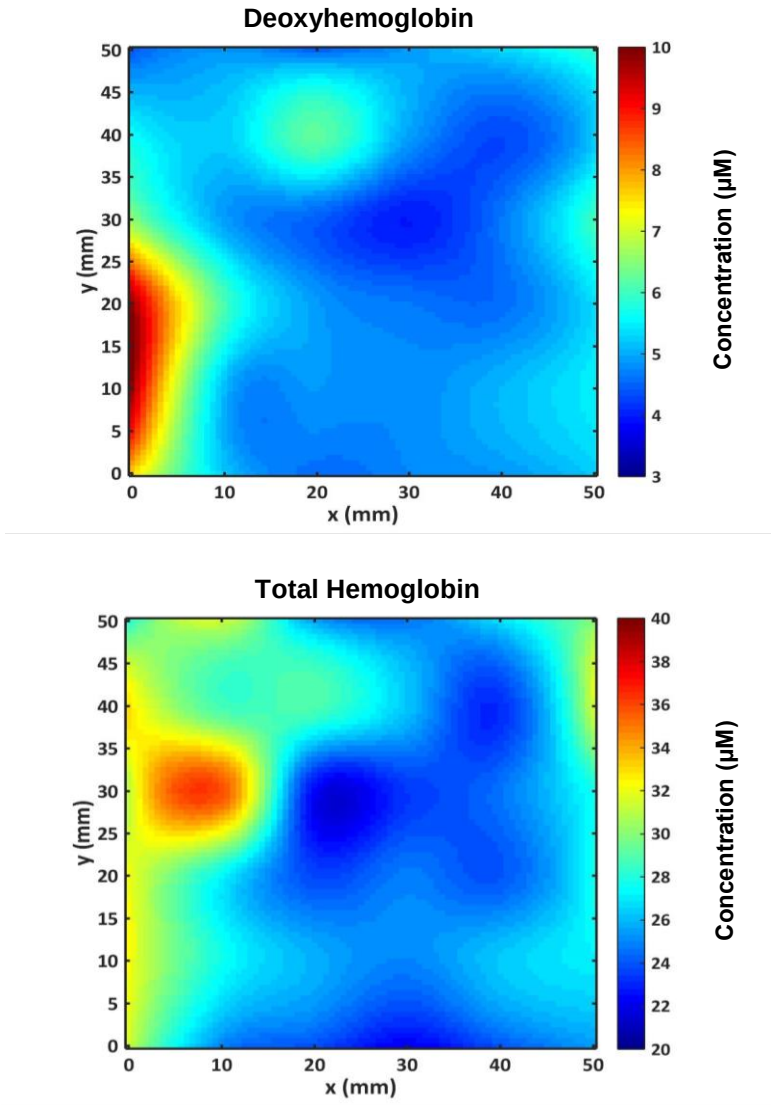

Figure 25. Chromophore concentrations in the right breast of a healthy volunteer measured using the dDOSI system. A quadrant of the areolar complex is located at the bottom left of the image.

Following the dDOSI breast measurements, an additional set of measurements was taken with a clinical DOSI system[30] developed by the Beckman Laser Institute, using the same measurement grid as was used in the

dDOSI measurements. Chromophore maps of resulting deoxyhemoglobin and total hemoglobin concentrations correlated well with those shown in Figure 25.

Conclusions and Future Work

The dDOSI system has been developed in order to increase access to patients by simplifying the standard benchtop DOSI system. The hardware-integrated dDOSI system utilizes direct digital signal generation and detection, which eliminates the need for a costly and cumbersome network analyzer. Laser diodes and current drivers can be miniaturized to further improve the portability of the system. The overall cost of the dDOSI (Appendix) system is nearly tenfold lower than that of the benchtop DOSI system, yet the accuracy and precision remain comparable to those of previous systems. By utilizing wavelength multiplexing, frequency sweep measurements can be taken at nearly 100 Hz, allowing for detection of physiological changes at the cardiac rate. These improvements to the DOSI platform will allow for more efficient patient measurements and the ability to comfortably measure patients in an infusion suite in order to ultimately optimize treatment regimens for those undergoing neoadjuvant chemotherapy.

Future work on the dDOSI system will involve implementing further stabilizing components on the PCBs that control the miniaturized laser diode driver modules in order to minimize transient voltage spikes. The fully miniaturized system with fiber-coupled laser diode modules will be rigorously tested to ensure reliability in clinical measurements.

The ability to take rapid frequency domain dDOSI measurements may allow for further investigation into hemodynamics, particularly examining

chromophore concentrations in abnormal tumor vasculature. Rapid measurements may also allow for future improvements in tissue scanning methods. Point scanning could be automated to improve speed and repeatability of chromophore map data acquisition.

Appendix. Cost of materials for fully miniaturized dDOSI system

Designation	Item	Part Number/ Manufacturer	Quantity	Unit Cost	Extended Cost
motherboard and components	MicroZed System-On-Module	Z7010	1	$199.00	$199.00
	4-Layer Motherboard PCB	Advanced Circuits	1	$283.45	$283.45
	4-Layer Frequency Synthesizer PCB	Advanced Circuits	6	$93.00	$558.00
	Direct Digital Synthesis Chips	AD9910	6	$56.93	$341.58
	Dual Channel 250MSPS ADC Chip	ADS62P49	1	$207.97	$207.97
	Remaining DDS Parts (Passives + Other ICs)		6	$30.00	$180.00
	Remaining ADC Parts (Passives + Other ICs)		1	$92.03	$92.03
	SD Card 2Gb		1	$5.99	$5.99
laser diodes	Pigtail laser - 658 nm	FMXL658-25YF0A	1	$394.00	$394.00
	Pigtail laser - 690 nm	FMXL690-25YF0A	1	$401.00	$401.00
	Pigtail laser - 785 nm	FMXL785-50YF0A	1	$434.00	$434.00
	Pigtail laser - 808 nm	FMXL808-50YF0B	1	$1,020.00	$1,020.00
	Pigtail laser - 830 nm	FMXL830-40YF0B	1	$459.00	$459.00
	Pigtail laser - 850 nm	FMXL850-40YF0B	1	$459.00	$459.00
current controllers	Laser diode drivers	LDD200-2P	6	$77.00	$462.00
	Custom PCB	Express PCB	1	$288.55	$288.55
	MOSFET	DMN2004DMKDICT-ND	6	$0.44	$2.64
	Op-amp	AD8032ARZ-REEL7CT-ND	6	$4.70	$28.21
	Capacitors	BC2665CT-ND	6	$0.18	$1.08
	Potentiometers	3386P-203LF-ND	6	$1.60	$9.60
	SMA connectors	WM9458-ND	6	$3.07	$18.43
	Additional connectors and passives (est.)		1	$50.00	$50.00
housing	Enclosure Box: Aluminum Black	Bud Industries	1	$122.00	$122.00
	Enclosure SMA Feed Through Connectors		8	$7.50	$60.00
	SMA Cables		6	$3.49	$20.94
	Grand Total				**$6,098.47**

References

[1] "National Cancer Institute: Surveillance, Epidemiology, and End Results Program." [Online]. Available: http://seer.cancer.gov/statfacts/html/breast.html. [Accessed: 01-May-2016].

[2] B. H. M. Kuerer, L. A. Newman, T. L. Smith, F. C. Ames, K. K. Hunt, K. Dhingra, R. L. Theriault, G. Singh, S. M. Binkley, N. Sneige, T. A. Buchholz, M. I. Ross, M. D. Mcneese, A. U. Buzdar, G. N. Hortobagyi, and S. E. Singletary, "Clinical Course of Breast Cancer Patients With Complete Pathologic Primary Tumor and Axillary Lymph Node Response to Doxorubicin-Based Neoadjuvant Chemotherapy," *J. Clin. Oncol.*, vol. 17, no. 2, pp. 460–469, 1999.

[3] M. Miller, R. A. Ottesen, J. C. Niland, L. Kruper, S. L. Chen, and C. Vito, "Tumor Response Ratio Predicts Overall Survival in Breast Cancer Patients Treated with Neoadjuvant Chemotherapy," *Ann. Surg. Oncol.*, vol. 21, pp. 3317–3323, 2014.

[4] A. S. Caudle, A. M. Gonzalez-Angulo, K. K. Hunt, P. Liu, L. Pusztai, W. F. Symmans, H. M. Kuerer, E. A. Mittendorf, G. N. Hortobagyi, and F. Meric-Bernstam, "Predictors of tumor progression during neoadjuvant chemotherapy in breast cancer," *J. Clin. Oncol.*, vol. 28, no. 11, pp. 1821–1828, 2010.

[5] P. Rastogi, S. J. Anderson, H. D. Bear, C. E. Geyer, M. S. Kahlenberg, A. Robidoux, R. G. Margolese, J. L. Hoehn, V. G. Vogel, S. R. Dakhil, D.

Tamkus, K. M. King, E. R. Pajon, M. J. Wright, J. Robert, S. Paik, E. P. Mamounas, and N. Wolmark, “Preoperative chemotherapy: Updates of national surgical adjuvant breast and bowel project protocols B-18 and B-27,” *J. Clin. Oncol.*, vol. 26, no. 5, pp. 778–785, 2008.

[6] M. J. Silverstein, A. Recht, M. D. Lagios, I. J. Bleiweiss, P. W. Blumencranz, T. Gizienski, S. E. Harms, J. Harness, R. J. Jackman, V. S. Klimberg, R. Kuske, G. M. Levine, M. N. Linver, E. A. Rafferty, H. Rugo, K. Schilling, D. Tripathy, P. W. Whitworth, and S. C. Willey, “Image-Detected Breast Cancer : State-of-the-Art Diagnosis and Treatment,” *ACS*, vol. 209, no. 4, pp. 504–520, 2009.

[7] J. Zakhireh, R. Gomez, and L. Esserman, “Converting evidence to practice : A guide for the clinical application of MRI for the screening and management of breast cancer,” *Eur. J. Cancer*, vol. 44, no. 18, pp. 2742–2752, 2008.

[8] H. Soliman, A. Gunasekara, M. Rycroft, J. Zubovits, and R. Dent, “Functional Imaging Using Diffuse Optical Spectroscopy of Neoadjuvant Chemotherapy Response in Women with Locally Advanced Breast Cancer,” vol. 16, no. 9, pp. 2605–2615, 2010.

[9] P. G. Anderson, J. M. Kainerstorfer, A. Sassaroli, N. Krishnamurthy, M. J. Homer, R. A. Graham, and S. Fantini, “Broadband optical mammography: Chromophore concentration and hemoglobin saturation contrast in breast cancer,” *PLoS One*, vol. 10, no. 3, pp. 1–23, 2015.

[10] A. Cerussi, D. Hsiang, N. Shah, R. Mehta, A. Durkin, J. Butler, and B. J.

Tromberg, “Predicting response to breast cancer neoadjuvant chemotherapy using diffuse optical spectroscopy.,” *Proc. Natl. Acad. Sci. U. S. A.*, vol. 104, no. 10, pp. 4014–4019, 2007.

[11] D. Roblyer, S. Ueda, A. Cerussi, W. Tanamai, A. Durkin, R. Mehta, D. Hsiang, J. a Butler, C. McLaren, W.-P. Chen, and B. Tromberg, “Optical imaging of breast cancer oxyhemoglobin flare correlates with neoadjuvant chemotherapy response one day after starting treatment.,” *Proc. Natl. Acad. Sci. U. S. A.*, vol. 108, no. 35, pp. 14626–14631, 2011.

[12] B. J. Tromberg, O. Coquoz, J. B. Fishkin, T. Pham, E. R. Anderson, J. Butler, M. Cahn, J. D. Gross, V. Venugopalan, and D. Pham, “Non-invasive measurements of breast tissue optical properties using frequency-domain photon migration.,” *Philos. Trans. R. Soc. Lond. B. Biol. Sci.*, vol. 352, no. 1354, pp. 661–668, 1997.

[13] B. J. Tromberg, L. Svaasand, T. Tsay, R. C. Haskell, and M. W. Berns, “Optical property measurements in turbid media using frequency domain photon migration,” *SPIE*, vol. 1525, pp. 52–58, 1991.

[14] A. Cerussi, “Diffuse Optical Spectroscopic Imaging (DOSI).” [Online]. Available: https://sites.google.com/site/dosiatbli/home. [Accessed: 10-May-2016].

[15] S. L. Jacques, “Optical properties of biological tissues : a review,” *Phys. Med. Biol.*, vol. 58, pp. R37–R61, 2013.

[16] J. Fishkin, E. Gratton, M. J. VandeVen, and W. W. Mantulin, “Diffusion of intensity modulated near-infrared light in turbid media,” *SPIE Proc.*, vol.

1431, pp. 122–135, 1991.

[17] T. H. Pham, O. Coquoz, I. Libraries, R. Libraries, B. J. Tromberg, and A. Solutions, “Broad bandwidth frequency domain instrument for quantitative tissue optical spectroscopy,” *Rev. Sci. Instrum.*, vol. 71, no. 6, pp. 83–100, 2000.

[18] R. C. Haskell, L. O. Svaasand, T. T. Tsay, T. C. Feng, M. S. McAdams, and B. J. Tromberg, “Boundary conditions for the diffusion equation in radiative transfer.,” *J. Opt. Soc. Am. A. Opt. Image Sci. Vis.*, vol. 11, no. 10, pp. 2727–41, 1994.

[19] U. J. Netz, J. Beuthan, and A. H. Hielscher, “Multipixel system for gigahertz frequency-domain optical imaging of finger joints,” *Rev. Sci. Instrum.*, vol. 79, pp. 1–14, 2008.

[20] T. D. O’Sullivan, A. E. Cerussi, D. J. Cuccia, and B. J. Tromberg, “Diffuse optical imaging using spatially and temporally modulated light,” *J. Biomed. Opt.*, vol. 17, no. 7, p. 071311, 2012.

[21] W. G. Zijlstra and A. Buursma, “Spectrophotometry of Hemoglobin: Absorption Spectra of Bovine Oxyhemoglobin, Deoxyhemoglobin, Carboxyhemoglobin, and Methemoglobin,” *Comp. Biochem. Physiol.*, vol. 118, no. 4, pp. 743–749, 1997.

[22] T. O. McBride, B. W. Pogue, S. Jiang, U. L. Österberg, and K. D. Paulsen, “A parallel-detection frequency-domain near-infrared tomography system for hemoglobin imaging of the breast in vivo,” *Rev. Sci. Instrum.*, vol. 72, no. 3, pp. 1817–1824, 2001.

[23] J. P. Culver, R. Choe, M. J. Holboke, L. Zubkov, T. Durduran, A. Slemp, V. Ntziachristos, B. Chance, and a G. Yodh, “Three-dimensional diffuse optical tomography in the parallel plane transmission geometry: evaluation of a hybrid frequency domain/continuous wave clinical system for breast imaging.,” *Med. Phys.*, vol. 30, no. 2, pp. 235–247, 2003.

[24] B. B. Zimmermann, Q. Fang, D. A. Boas, and S. A. Carp, “Frequency domain near-infrared multiwavelength imager design using high-speed, direct analog-to-digital conversion,” *J. Biomed. Opt.*, vol. 21, no. 1, p. 016010, 2016.

[25] G. Yu, T. Durduran, D. Furuya, J. H. Greenberg, and A. G. Yodh, “Frequency-domain multiplexing system for in vivo diffuse light measurements of rapid cerebral hemodynamics,” *Appl. Opt.*, vol. 42, no. 16, pp. 2931–2939, 2003.

[26] U. M. Weigel, R. B. Revilla, N. H. Oliverio, A. A. González, J. C. Cifuentes, P. Zirak, R. Saiz, D. Mitrani, J. Ninou, O. Casellas, and T. Durduran, “A new, modular frequency domain diffuse optical monitor in the digital domain,” in *Biomedical Optics and 3D Imaging OSA*, 2012.

[27] B. Pogue, M. Testorf, T. McBride, U. Osterberg, and K. Paulsen, “Instrumentation and design of a frequency-domain diffuse optical tomography imager for breast cancer detection.,” *Opt. Express*, vol. 1, no. 13, pp. 391–403, 1997.

[28] Y. S. Yang, H. L. Liu, X. D. Li, and B. Chance, “Low-cost frequency-domain photon migration instrument for tissue spectroscopy, oximetry, and

imaging," *Opt. Eng.*, vol. 36, no. 5, pp. 1562–1569, 1997.

[29] S. J. Madsen, E. R. Anderson, R. C. Haskell, and B. J. Tromberg, "Keywords : frequency-domain photon migration , optical properties , diode laser , network analyzer ," in *SPIE*, 1995, vol. 2389, pp. 257–263.

[30] K.-S. No, R. Kwong, P. H. Chou, and A. Cerussi, "Design and testing of a miniature broadband frequency domain photon migration instrument.," *J. Biomed. Opt.*, vol. 13, no. 5, p. 050509, 2009.

[31] D. Roblyer, T. D. O'Sullivan, R. V Warren, and B. Tromberg, "Feasibility of Direct Digital Sampling for Diffuse Optical Frequency Domain Spectroscopy in Tissue.," *Meas. Sci. Technol.*, vol. 24, no. 4, p. 045501, 2013.

[32] J. Jung, R. Istfan, and D. Roblyer, "Note: A simple broad bandwidth undersampling frequency-domain digital diffuse optical spectroscopy system," *Rev. Sci. Instrum.*, vol. 85, no. 7, pp. 72–75, 2014.

[33] J. M. Bland and D. G. Altman, "Statistical methods for assessing agreement between two methods of clinical measurement," *Int. J. Nurs. Stud.*, vol. 47, no. 8, pp. 931–936, 2010.

[34] N. Shah, A. E. Cerussi, D. Jakubowski, D. Hsiang, J. Butler, and B. J. Tromberg, "Spatial variations in optical and physiological properties," *J. Biomed. Opt.*, vol. 9, no. 3, pp. 534–540, 2004.

[35] J. Yong, A. Foo, and C. S. Lim, "PULSE TRANSIT TIME BASED ON PIEZOELECTRIC," *J. Clin. Monit. Comput.*, vol. 20, pp. 185–192, 2006.

Curriculum Vitae

Alyssa Torjesen
YOB: 1988

Affiliation: Boston University, College of Engineering
Department of Biomedical Engineering

44 Cummington Street
Boston, MA 02215
Email: torjesen@bu.edu
Phone: 978-317-3139

EDUCATION

Boston University
Boston, MA
M.S. Biomedical Engineering (In progress)

Pepperdine University
Malibu, CA
B.S. Physics, 2010
B.A. Spanish, 2010

EXPERIENCE

Boston University—Biomedical Optical Technologies Lab
Research Assistant
2015-Present

Academic Approach
Tutor
2011-Present

Cardiovascular Engineering, Inc.
Research Assistant
2011-2015

Aston English School (Taiyuan, China)
Foreign English Teacher
2010-2011

PUBLICATIONS

1. Woodard, T; Sigurdsson, S; Gotal, JD; **Torjesen, AA**; Inker, L; Aspelund, T; Eiriksdottir, G; Gudnason, V; Harris, TB; Launer, LJ; Levey, AS; Mitchell, GF. Segmental kidney volumes measured by dynamic contrast-enhanced magnetic resonance imaging and their association with CKD in older people. *Am J Kidney Dis*. 2015:65:41-48.

2. Bell, V; Sigurdsson, S; Westenberg, JJ; Gotal, JD; **Torjesen, AA**; Aspelund, T; Launer, LJ; Harris, TB; Gudnason, V; de Roos, A; Mitchell, GF. Relations between aortic stiffness and left ventricular structure and function in older people in the Age, Gene/Environment Susceptibility—Reykjavik Study. *Circ Cardiovasc Imaging*. 2015:8:e003039.

3. **Torjesen, AA**; Sigurðsson, S; Westenberg, JJM; Gotal, JD; Bell, V; Aspelund, T; Launer, LJ; de Roos, A; Gudnason, V; Harris, TB; Mitchell, GF. Pulse pressure relation to aortic structure and left ventricular coupling in older people in the community-based AGES-Reykjavik Study. 2014. *Hypertension*. 2014;64:756-761.

4. **Torjesen, AA**; Wang, N; Larson, MG; Hamburg, NM; Vita, JA; Levy, D; Benjamin, EJ; Vasan, RS; Mitchell, GF. Forward and backward wave morphology and central pressure augmentation in men and women in the Framingham Heart Study. Hypertension. 2014;64:259-265.

5. Woodard, T; Sigurdsson, S; Gotal, JD; **Torjesen, AA**; Inker, LA; Aspelund, T; Eiriksdottir, G; Gudnason, V; Harris, TB; Launer, LJ; Levey, AS; Mitchell, GF. Mediation analysis of aortic stiffness and renal microvascular function. JASN. 2014;25:1869-1882.

PRESENTATIONS

1. **Torjesen, A**.*, Istfan, R., Peterson, H., Roblyer, D. An Ultra-Fast Digital Diffuse Optical Spectroscopic Imaging (dDOSI) System for Monitoring Chemotherapy Response. OSA Biomedical Optics. Ft. Lauderdale, FL. April 2016.

2. Bell, V*; Westenberg, JJM; Aspelund, T; Gudnason, V; Mitchell, WA; Gotal, JD; Launer, LJ; Sigurðsson, S; **Torjesen, AA**; de Roos, A; Harris, TB; Mitchell, GF. Longitudinal and circumferential strain of the proximal aorta. Poster presentation. North American Artery Meeting. Chicago, Il; September, 2014.

3. Woodard, T*; Sigurdsson, S; Gotal, JD; **Torjesen, AA**; Inker, L; Aspelund, T; Eiriksdottir, G; Gudnason, V; Harris, T; Launer, LJ; Levey, AS; Mitchell, GF. Kidney magnetic resonance imaging reveals structural abnormalities that are associated with kidney function and risk factors for adverse outcomes in an older community-based cohort. Poster presentation. American Society of Nephrology Kidney Week. Atlanta, GA; November, 2013.

4. **Torjesen, AA***. Higher pulse pressure in older people is associated with smaller aortic lumen area. Oral presentation. Icelandic Heart Association Investigators Meeting. Kopavagor, Iceland; April, 2012.

5. **Torjesen, AA***; Thomasma, B*. Language, Landscape and the Making of Global Citizens. Oral presentation. Pepperdine Undergraduate Research Banquet. Malibu, CA; February, 2010.

* Denotes presenter(s)